

Sequential transport maps using SoS density estimation and α -divergences

Benjamin Zanger*, Tiangang Cui†, Martin Schreiber‡, Olivier Zahm§

February 29, 2024

Abstract

Transport-based density estimation methods are receiving growing interest because of their ability to efficiently generate samples from the approximated density. We further investigate the sequential transport maps framework proposed from [10, 11], which builds on a sequence of composed Knothe-Rosenblatt (KR) maps. Each of those maps are built by first estimating an intermediate density of moderate complexity, and then by computing the exact KR map from a reference density to the precomputed approximate density. In our work, we explore the use of Sum-of-Squares (SoS) densities and α -divergences for approximating the intermediate densities. Combining SoS densities with α -divergence interestingly yields *convex* optimization problems which can be efficiently solved using semidefinite programming. The main advantage of α -divergences is to enable working with *unnormalized* densities, which provides benefits both numerically and theoretically. In particular, we provide two new convergence analyses of the sequential transport maps: one based on a triangle-like inequality and the second on information geometric properties of α -divergences for unnormalized densities. The choice of intermediate densities is also crucial for the efficiency of the method. While tempered (or annealed) densities are the state-of-the-art, we introduce diffusion-based intermediate densities which permits to approximate densities known from samples only. Such intermediate densities are well-established in machine learning for generative modeling. Finally we propose and try different low-dimensional maps (or lazy maps) for dealing with high-dimensional problems and numerically demonstrate our methods on several benchmarks, including Bayesian inference problems and unsupervised learning task.

1 Introduction

Density estimation is a fundamental problem in data sciences. Transport-based methods are receiving growing interest because of their ability to sample easily from the approx-

*Université Grenoble Alpes, Inria, CNRS, Grenoble INP, LJK, 38000 Grenoble, France (benjamin.zanger@inria.fr)

†School of Mathematics and Statistics, University of Sydney, NSW 2006, Australia (tiangang.cui@sydney.edu.au)

‡Université Grenoble Alpes, LJK, 38000 Grenoble, France
Technical University of Munich, Germany (martin.schreiber@univ-grenoble-alpes.fr)

§Université Grenoble Alpes, Inria, CNRS, Grenoble INP, LJK, 38000 Grenoble, France (olivier.zahm@inria.fr)

imated density [26, 18, 31, 34]. These methods aim at building a deterministic diffeomorphism \mathcal{T} , also called a transport map, which pushes forward an arbitrary reference probability density ρ_{ref} to a given target probability density π to be approximated. This pushforward density, denoted by $\mathcal{T}_{\#}\rho_{\text{ref}}$, is the density of the random vector $\mathcal{T}(\Xi)$, where $\Xi \sim \rho_{\text{ref}}$. Variational methods consist in solving a problem of the form

$$\min_{\mathcal{T} \in \mathcal{M}} D(\pi || \mathcal{T}_{\#}\rho_{\text{ref}}), \quad (1)$$

where the statistical divergence $D(\cdot || \cdot)$ and the set of diffeomorphisms \mathcal{M} are typically chosen so that problem (1) is a tractable problem. Typically, the Kullback-Leibler (KL) divergence is employed for $D(\cdot || \cdot)$ when only samples from π are available (learning from data), while the reverse KL divergence is utilized when π can be evaluated up to a normalizing constant (learning from unnormalized density). Minimizing the reverse KL divergence, however, fails to capture multi-modal densities π , a well known problem for such zero-forcing divergence, see e.g. [5, 29, 16]. Regarding the set \mathcal{M} , the first cornerstone for handling high-dimensional diffeomorphic maps is the monotone triangular map, where each i -th map component depends on the first i variables only and is monotone in the i -th variable [3, 19, 14]. As to increase the approximation power, the second cornerstone is to compose multiple monotone triangular map. This is the basic idea of many map parametrization used in the Normalizing flows literature [30, 16, 34] to cite just a few. Let us emphasize that, in principle, there exists infinitely many maps \mathcal{T} which satisfy $\mathcal{T}_{\#}\rho_{\text{ref}} = \pi$. This is contrarily to the Monge optimal transport problem which seeks the map \mathcal{T} that minimizes some transport-related loss $\int (\mathbf{x} - \mathcal{T}(\mathbf{x}))^2 d\rho_{\text{ref}}(\mathbf{x})$ under the constraint $\mathcal{T}_{\#}\rho_{\text{ref}} = \pi$, see [43, 32]. Instead, the goal of (1) is to build *a tractable* map $\mathcal{T} \in \mathcal{M}$ such that $\mathcal{T}_{\#}\rho_{\text{ref}} \approx \pi$. In other terms, problem (1) is not concerned with the paths by which \mathcal{T} transports ρ_{ref} to π ; it solely focuses on the resulting distance between $\mathcal{T}_{\#}\rho_{\text{ref}}$ and π .

An emerging strategy for solving (1) is to first approximate π with an approximate density $\tilde{\pi}$ and then to compute a map \mathcal{T} which exactly pushes forward ρ_{ref} to $\tilde{\pi}$. Among the infinitely many maps \mathcal{T} which satisfy $\mathcal{T}_{\#}\rho_{\text{ref}} = \tilde{\pi}$, the Knothe-Rosenblatt (KR) map is rather simple to evaluate since it requires only computing the conditional marginals of $\tilde{\pi}$. In the seminal work [15], $\tilde{\pi}$ is built in the tensor-train format, an approximation class which permits to efficiently compute the KR map, see also [8, 10, 9]. Polynomial approximation methods have also been used recently in [11, 44] for building transport maps. In all these papers, the statistical divergence $D(\cdot || \cdot)$ is chosen to be the Hellinger distance, which is the L^2 distance between square root densities. Conveniently, this distance permits building approximations $\tilde{\pi}$ to π using standard L^2 function approximation techniques, like polynomial interpolation, least-squares or tensor methods. In general, however, the variational problem $\min_{\tilde{\pi}} D(\pi || \tilde{\pi})$ is difficult to solve when π is multimodal or when it concentrates on a low-dimensional manifold. The solution proposed in [8] consists in introducing an arbitrary sequence of bridging densities

$$\pi^{(1)}, \pi^{(2)}, \dots, \pi^{(L)} = \pi, \quad (2)$$

with increasing complexity. Similar to Sequential Monte Carlo Samplers [12], this sequence allows for breaking down the challenging approximation problem (1) into a sequence of intermediate problems of more manageable complexity. A classical choice of bridging densities are tempered densities $\pi^{(\ell)}(\mathbf{x}) \propto \pi(\mathbf{x})^{\beta_{\ell}}$ with parameters $0 \leq \beta_0 \leq \dots \leq \beta_L = 1$ [8, 11, 10], although other options are possible depending on the application

[9, 13]. In practice, the strategy consists in building L transport maps $\mathcal{Q}_1, \dots, \mathcal{Q}_L$ one after the other by solving the following variational problems sequentially

$$\min_{\mathcal{Q}_\ell \in \mathcal{M}} D(\pi^{(\ell)} \| (\mathcal{T}_{\ell-1} \circ \mathcal{Q}_\ell)_\# \rho_{\text{ref}}), \quad \text{where } \mathcal{T}_{\ell-1} = \mathcal{Q}_1 \circ \dots \circ \mathcal{Q}_{\ell-1}. \quad (3)$$

These problems are equivalent to estimating the pullback density $(\mathcal{T}_{\ell-1})^\# \pi^{(\ell)}$ with an intermediate approximation $\rho^{(\ell)} = (\mathcal{Q}_\ell)_\# \rho_{\text{ref}}$. Again, this can be done by first building the approximate density $\rho^{(\ell)}$ and then by extracting the KR map \mathcal{Q}_ℓ which pushes forward ρ_{ref} to the precomputed $\rho^{(\ell)}$. An illustration of such an sequential approximation using $L = 3$ steps is depicted in Figure 1.

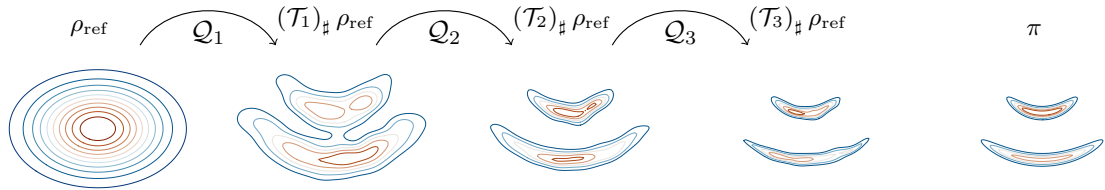


Figure 1: Visualization of the approximation of a bimodal distribution π (right) using $L = 3$ intermediate tempered densities estimated using SoS (4) and a gaussian reference distribution ρ_{ref} .

In this paper, we pursue the above methodology by extending it to Sum-of-Squares (SoS) density estimation using α -divergences. In details, we construct the each intermediate density $\rho^{(\ell)}$ under the form

$$\rho^{(\ell)}(\mathbf{x}) \propto (\Phi(\mathbf{x})^\top A_\ell \Phi(\mathbf{x})) \rho_{\text{ref}}(\mathbf{x}), \quad (4)$$

where $A_\ell \succeq 0$ is a positive semidefinite matrix to be determined, and Φ is a vectorization of orthonormal basis function. This approximation class (4) is a generalization of the polynomial squared method used in [11, 44] where $\rho^{(\ell)}(\mathbf{x}) \propto (v_\ell^\top \Phi(\mathbf{x}))^2 \rho_{\text{ref}}(\mathbf{x})$. SoS densities also permit to efficiently compute the KR map \mathcal{Q}_ℓ such that $(\mathcal{Q}_\ell)_\# \rho_{\text{ref}} = \rho^{(\ell)}$, which is a crucial property for the proposed methodology. SoS functions have also been used in [19, 37] for parametrizing the map \mathcal{T} directly in order to ensure the monotonicity of each map components. Contrarily to the previous works which, depending on the application, utilize either the Hellinger distance, the KL divergence or the reverse KL divergence, we here employ the class of α -divergences $D_\alpha(\cdot \| \cdot)$ with parameter $\alpha \in \mathbb{R}$. This class of divergence encompasses all the previously mentioned divergences and, consequently, permits to unify the convergence analysis for problem (3). Using the notion of α -geodesic, we also propose a novel convergence analysis for (3) which relies on the geometry induced by $D_\alpha(\cdot \| \cdot)$. Most importantly, the use of α -divergence for learning SoS densities (4) results in a *convex* optimization problems for (3) which can be efficiently solved using off-the-shelf toolboxes. This unified framework we propose enables estimation of the density π not only from data (when only samples from π are available) but also from point-evaluations of the unnormalized density π .

Finally, we explore different ways to define the sequence of bridging densities (2). When learning from data, we rather consider the following bridging densities defined by convoluting π with a diffusion kernel $\kappa_t(\cdot, \cdot)$, that is

$$\pi^{(\ell)}(\mathbf{x}) = \int \kappa_{t_\ell}(\mathbf{x}, \mathbf{y}) \pi(\mathbf{y}) d\mathbf{y}. \quad (5)$$

with time parameter $\infty = t_0 \geq t_1 \geq \dots \geq t_L = 0$. The main reason for employing (5) is that samples from $\pi^{(\ell)}$ are readily obtained by simulating an Ornstein-Uhlenbeck process. This idea is at the root of diffusion models [39, 40].

We introduce α -divergences and SoS functions in Section 2 and 3. We then explain diffusion bridging densities and provide convergence analysis of sequential transport maps in Section 4. To address the curse of dimensionality, in Section 5 we give two methods to scale to higher dimensions. Finally, in Section 6, numerical examples demonstrate the feasibility of the proposed methods.

2 Variational density estimation using α -divergence

We propose to use α -divergences [5] for the variational density estimation. Using the definition of α -divergences from [45], for a given $\alpha \in \mathbb{R}$, the α -divergence between two unnormalized densities f and g (meaning integrable and positive functions) reads

$$D_\alpha(f||g) = \int \phi_\alpha\left(\frac{f(\mathbf{x})}{g(\mathbf{x})}\right) g(\mathbf{x}) d\mathbf{x}, \quad \text{with } \phi_\alpha(t) = \begin{cases} \frac{t^\alpha - 1}{\alpha(\alpha - 1)} - \frac{t - 1}{\alpha - 1} & \alpha \notin \{0, 1\} \\ t \log(t) - t + 1 & \alpha = 1 \\ -\log(t) + t - 1 & \alpha = 0. \end{cases} \quad (6)$$

Notice that for all $\alpha \in \mathbb{R}$, the function $\phi_\alpha : \mathbb{R}_{\geq 0} \rightarrow \mathbb{R}_{\geq 0}$ is positive, convex $\phi_\alpha''(t) > 0$, and is minimal at $t = 1$, meaning $\phi_\alpha'(1) = 0$. Denoting by $\pi_f(\mathbf{x}) \propto f(\mathbf{x})$ and $\pi_g(\mathbf{x}) \propto g(\mathbf{x})$ the probability densities obtained by normalizing respectively f and g , the choices $\alpha \in \{0, 1/2, 1, 2\}$ yield respectively to

$$D_1(\pi_f||\pi_g) = D_{\text{KL}}(\pi_f||\pi_g), \quad D_0(\pi_f||\pi_g) = D_{\text{KL}}(\pi_g||\pi_f), \quad (7)$$

$$D_{1/2}(\pi_f||\pi_g) = 4 D_{\text{Hell}}(\pi_f||\pi_g)^2, \quad D_2(\pi_f||\pi_g) = \frac{1}{2} \chi^2(\pi_f||\pi_g), \quad (8)$$

where $D_{\text{KL}}(\pi_f||\pi_g) = \int \log\left(\frac{\pi_f}{\pi_g}\right) d\pi_f$ is the Kullback-Leibler divergence, $D_{\text{Hell}}(\pi_f||\pi_g) = \left(\frac{1}{2} \int (\sqrt{\pi_f} - \sqrt{\pi_g})^2 d\mathbf{x}\right)^{1/2}$ the Hellinger distance and $\chi^2(\pi_f||\pi_g) = \int \left(\frac{\pi_f}{\pi_g} - 1\right)^2 d\pi_g$ the chi-square divergence.

One practical advantage of using α -divergences with *unnormalized* density functions is that there is no need to enforce the approximate density to integrate to one while learning it. Additionally, one avoid the requirement of knowing the normalizing constant of the target density, which is convenient for Bayesian inverse problems where the posterior density is known up to a multiplicative constant. For instance, it is shown in [16] that a direct discretization of the KL divergence (for probability densities) might not converge well: in Appendix B, we show that the discretization of $D_1(f||g)$ (the extension of the KL divergence for unnormalized measures) does not suffer from this instability and also refer to [28, Appendix A] in which the same issue is shown for discretization of f-divergences. Denoting by $Z_f = \int f(\mathbf{x}) d\mathbf{x}$ and $Z_g = \int g(\mathbf{x}) d\mathbf{x}$ the normalizing constant of f and g , we show in Appendix A.3 that

$$D_\alpha(f||g) = \frac{Z_f^\alpha}{Z_g^{\alpha-1}} D_\alpha(\pi_f||\pi_g) + Z_g \phi_\alpha\left(\frac{Z_f}{Z_g}\right), \quad (9)$$

holds for any unnormalized densities f, g . This relation suggests that for a density f , minimizing $g \mapsto D_\alpha(f||g)$ permits to control both $D_\alpha(\pi_f||\pi_g)$ and $\phi_\alpha\left(\frac{Z_f}{Z_g}\right)$ so that, after normalizing g , the probability density π_g yields a controlled approximation to π_f .

According to [27], minimizing $g \mapsto D_\alpha(f||g)$ with $\alpha \leq 0$ forces $g(\mathbf{x}) \ll 1$ in regions where $f(\mathbf{x}) \ll 1$, thus avoiding *false positives* (zero forcing property). Reciprocally, minimizing $g \mapsto D_\alpha(f||g)$ with $\alpha \gg 1$ forces $g(\mathbf{x}) \gg 1$ in regions where $f(\mathbf{x}) \gg 1$, which avoids *false negatives* (zero avoiding property). This is coherent with the duality property

$$D_\alpha(f||g) = D_{1-\alpha}(g||f), \quad (10)$$

which holds for any $\alpha \in \mathbb{R}$, see e.g. [1]. Another fundamental property of α -divergences is the stability under transportation by a diffeomorphism \mathcal{T} , meaning

$$D_\alpha(f||\mathcal{T}_\#g) = D_\alpha(\mathcal{T}^\#f||g). \quad (11)$$

As detailed later in Section 4, this property permits us to reformulate problem (3) as an approximation of $\mathcal{T}_{\ell-1}^\#\pi^{(\ell)}$, the pullback of the ℓ -th bridging density via the map $\mathcal{T}_{\ell-1}$. For the sake of completeness, the derivation of Equation (11) is given in Appendix A.2.

In practice, we distinguish the cases where either the target probability density π can be evaluated up to a normalizing constant, or where the target probability density is only known via samples from π . The first case typically corresponds to Bayesian inverse problems, where the goal is to sample from the posterior density

$$\pi(\mathbf{x}) \propto f(\mathbf{x}) := \mathcal{L}(\mathbf{x}, y)\pi_0(\mathbf{x}). \quad (12)$$

Here, π_0 denotes the prior and $\mathcal{L}(\mathbf{x}, y)$ the likelihood of a given data set y conditioned on \mathbf{x} . A related application is rare event estimation where $\mathcal{L}(\mathbf{x}, y)$ is the indicator function (of level y) of the event which we need to compute the probability of. One can use a Monte-Carlo estimation of $D_\alpha(f||g)$ of the form of

$$\widehat{D}_\alpha(f||g) = \frac{1}{N} \sum_{i=1}^N \phi_\alpha \left(\frac{f(\mathbf{X}^{(i)})}{g(\mathbf{X}^{(i)})} \right) \frac{g(\mathbf{X}^{(i)})}{\rho_{\text{ref}}(\mathbf{X}^{(i)})}, \quad (13)$$

where $\mathbf{X}^{(1)}, \dots, \mathbf{X}^{(N)} \sim \rho_{\text{ref}}$ are independent samples drawn from a given reference measure ρ_{ref} . We discuss later in Section 3.3 the choice of ρ_{ref} .

Property 1 (Convexity of α -divergence). The function $t \mapsto t\phi_\alpha(u/t)$ is convex for any $\alpha \in \mathbb{R}$ and $u \in \mathbb{R}_{\geq 0}$. As a consequence, the functions $g \mapsto D_\alpha(f||g)$ and $g \mapsto \widehat{D}_\alpha(f||g)$ are also convex.

In the case where only samples from π are known, setting $\alpha = 1$ yields the KL divergence $D_{\text{KL}}(\pi||\pi_g) = \int \log(\pi) d\pi - \int \log(\pi_g) d\pi$. A Monte-Carlo estimate of the last term yields

$$\widehat{\mathcal{J}}_{\text{KL}}(\pi_g) = -\frac{1}{N} \sum_{i=1}^N \log(\pi_g(\mathbf{X}^{(i)})), \quad (14)$$

where here $\mathbf{X}^{(1)}, \dots, \mathbf{X}^{(N)}$ are samples from π . Note that $\pi_g \mapsto \widehat{\mathcal{J}}_{\text{KL}}(\pi_g)$ is also convex over the set of probability measures π_g .

3 Sum-of-Squares densities

Let $\{\phi_1, \dots, \phi_m\}$ be a family of m functions in $L^2_{\rho_{\text{ref}}}(\mathcal{X})$, where $\mathcal{X} \subset \mathbb{R}^d$ is the support of a reference density ρ_{ref} . Given a symmetric positive semidefinite matrix $A \succeq 0$ in $\mathbb{R}^{m \times m}$, we introduce the Sum-of-Squares (SoS) functions as

$$g_A(\mathbf{x}) = (\Phi(\mathbf{x})^\top A \Phi(\mathbf{x})) \rho_{\text{ref}}(\mathbf{x}), \quad (15)$$

where $\Phi(\mathbf{x}) = (\phi_1(\mathbf{x}), \dots, \phi_m(\mathbf{x}))$. By construction, $g_A : \mathcal{X} \rightarrow \mathbb{R}_+$ is positive and integrable. Indeed, denoting by $A = \sum_{i=1}^m \lambda_i u_i u_i^\top$ the eigenvalue decomposition of A with $\lambda_i \geq 0$ and $u_i \in \mathbb{R}^m$, the function $\mathbf{x} \mapsto \Phi(\mathbf{x})^\top A \Phi(\mathbf{x}) = \sum_{i=1}^m \lambda_i (u_i^\top \Phi(\mathbf{x}))^2$ is the sum of m squared functions, which explains the terminology SoS. Note that g_A does not necessarily integrate to one. We call SoS functions which integrate to one SoS *densities* and introduce them in Section 3.3. Since the parametrization $A \mapsto g_A$ is linear, the function $A \mapsto \widehat{D}_\alpha(f||g_A)$ as in (13) remains convex, as first mentioned in [25]. The resulting convex problem $\min_{A \succeq 0} \widehat{D}_\alpha(f||g_A)$ can be efficiently solved by using semidefinite programming (SDP). Toolboxes to solve such problems computationally are for example *JuMP.jl* [24] and *CVX* [17].

Next in Section 3.1 we describe how to construct Φ using orthonormal basis function. In Section 3.2 we show how to efficiently perform integration of SoS densities. Finally in Section 3.3 we show how to compute the Knothe-Rosenblatt map of a SoS probability density.

Remark 3.1. While $A \succeq 0$ is sufficient to ensure the positivity of g_A , this condition can be relaxed depending on \mathcal{X} and Φ . For instance, for polynomial basis Φ and a semi-algebraic set \mathcal{X} , the condition $A \succeq 0$ can be replaced with a weaker *moment-sequence condition*, for example see [22, 33]. This is, however, not considered in the present paper.

3.1 Tensor product basis

Assuming $\mathcal{X} = \mathcal{X}_1 \times \dots \times \mathcal{X}_d$ is a product space and $\rho_{\text{ref}}(\mathbf{x}) = \rho_{\text{ref}_1}(x_1) \dots \rho_{\text{ref}_d}(x_d)$ a product measure, we can construct $\Phi : \mathcal{X} \rightarrow \mathbb{R}^m$ by tensorizing univariate orthonormal functions as follow. Let $\{\phi_i^k\}_{i=1}^\infty$ be a set of orthonormal functions on $L^2_{\rho_{\text{ref}_k}}(\mathcal{X}_k)$, $1 \leq k \leq d$ and, given a multi-index $\alpha \in \mathbb{N}^d$, consider the following tensorization

$$\phi_\alpha(\mathbf{x}) = \phi_{\alpha_1}^1(x_1) \dots \phi_{\alpha_d}^d(x_d).$$

Then $\{\phi_\alpha\}_{\alpha \in \mathbb{N}^d}$ forms an orthonormal basis of $L^2_{\rho_{\text{ref}}}(\mathcal{X})$. In our work, we use multivariate polynomials to define ϕ_α although, in principle, any set of orthonormal functions on $L^2_{\rho_{\text{ref}_k}}(\mathcal{X}_k)$ can be used (trigonometric functions, wavelets,...). In the following, we give examples of orthogonal bases, including Legendre polynomial on $[-1, 1]$, Hermite polynomials on \mathbb{R} , and transformed Legendre polynomials on generic domains.

Example 1 (Orthogonal polynomials). A property of any orthogonal polynomials basis $\{P_n\}_{n \geq 0}$ in $L^2_{\rho_{\text{ref}}}$ is that they can be computed efficiently via a recurrence relation, given by

$$P_n(x) = (a_n x + b_n) P_{n-1}(x) + c_n P_{n-2}(x), \quad (16)$$

where the series a_n, b_n , and c_n depend on ρ_{ref} [21]. For the uniform density $\rho_{\text{ref}} = \mathcal{U}([-1, 1])$ on the bounded domain $[-1, 1]$, we obtain the Legendre polynomials with

$$a_n = \frac{2n+1}{n+1} \quad b_n = 0 \quad c_n = \frac{n}{n+1}. \quad (17)$$

The normalized Legendre polynomials L_n are obtained by

$$L_n(x) = \sqrt{n + \frac{1}{2}} P_n(x). \quad (18)$$

For the Gaussian measure $\rho_{\text{ref}} = \mathcal{N}(0, 1)$, on the unbounded domain \mathbb{R} , we obtain the probabilist's Hermite polynomials $H_n(x)$ with the recurrence relation

$$a_n = 1 \quad b_n = 0 \quad c_n = -n. \quad (19)$$

Using univariate Hermite polynomials for Φ , it is assured that $\lim_{x \rightarrow \infty} f_A(x)\omega(x) = 0$ and that the integral $\int_{-\infty}^{\infty} f_A(x)\omega(x)dx < \infty$ for $\omega(x) = \exp(-x^2/2)$. However, for numerical reasons, we prefer to use transformed Legendre polynomials when working in \mathbb{R}^d , which we explain in the next example.

Example 2 (Transformed Legendre polynomials [38]). Another way to obtain an orthogonal univariate basis of $L_{\rho_{\text{ref}}}^2(\mathcal{X})$ is to consider Legendre polynomials L_n on $L_{\mu}^2([-1, 1])$ with $\mu = \mathcal{U}([-1, 1])$ and the map \mathcal{R} such that $\mathcal{R}_{\#}\mu = \rho_{\text{ref}}$. From the normalized Legendre polynomials $\{L_i\}_{i \geq 0}$ we can create functions $\{\phi_i\}_{i \geq 0}$ given by

$$\phi_i(x) = L_i(\mathcal{R}^{-1}(x)) \quad (20)$$

which are orthonormal in $L_{\rho_{\text{ref}}}^2(\mathcal{X})$,

$$\int \phi_i(x)\phi_j(x) \rho_{\text{ref}}(x)dx = \int \phi_i(\mathcal{R}(x'))\phi_j(\mathcal{R}(x'))\mathcal{R}_{\#}\rho_{\text{ref}}(x')dx' \quad (21)$$

$$= \int L_i(x')L_j(x')\mu(x')dx' = \delta_{i,j}. \quad (22)$$

We show two transformations from [11] and [38] to transform Legendre polynomials to orthogonal functions on \mathbb{R} in the following table.

	$\mathcal{R}(x)$	$ \nabla\mathcal{R}(x) $	$\mathcal{R}^{-1}(x)$	$ \nabla\mathcal{R}^{-1}(x) $
logarithmic	$\tanh(x)$	$1 - \tanh(x)^2$	$\frac{1}{2} \log\left(\frac{1+x}{1-x}\right)$	$\frac{1}{1-x^2}$
algebraic	$\frac{x}{\sqrt{1+x^2}}$	$\frac{1}{(1+x^2)^{3/2}}$	$\frac{x}{\sqrt{1-x^2}}$	$\frac{1}{(1-x^2)^{3/2}}$

In practice, we work with a subset of indices $\mathcal{K} \subset \mathbb{N}^d$ with finite cardinality $|\mathcal{K}| = m$. In our implementation we use

$$\mathcal{K} = \left\{ \alpha \in \mathbb{N}^d : \sum_{i=1}^d \alpha_i \leq p \right\}, \quad m = \binom{p+d}{d}, \quad (23)$$

which yields the set of polynomials of total degree bounded by p . In order to vectorize $\{\phi_{\alpha}(\mathbf{x})\}_{\alpha \in \mathcal{K}}$ in a vector $\Phi(\mathbf{x}) \in \mathbb{R}^m$, we consider a bijective map

$$\sigma : \mathcal{K} \rightarrow \{1, \dots, m\},$$

which lists the elements of \mathcal{K} in the lexicographical order. Other sets are possible, *e.g.* downward closed sets which allow for adaptivity, see [7]. We then define the feature map $\Phi : \mathbb{R}^d \rightarrow \mathbb{R}^m$ such that $\Phi_i(\mathbf{x}) = \phi_{\sigma^{-1}(i)}(\mathbf{x})$.

3.2 Integration of SoS functions

Let us rewrite the SoS functions from Eq. (15) to the form $g_A(\mathbf{x}) = \text{trace}(A\Phi(\mathbf{x})\Phi(\mathbf{x})^\top \rho_{\text{ref}}(\mathbf{x}))$. This allows to apply linear operators \mathcal{L} acting on functions of \mathbf{x} , such as integration and differentiation, to $\Phi(\mathbf{x})\Phi(\mathbf{x})^\top \rho_{\text{ref}}(\mathbf{x})$ as follow (also see [25])

$$\mathcal{L}g_A(\mathbf{x}) = \text{trace}(AW(\mathbf{x})), \quad \text{where } W(\mathbf{x}) = \mathcal{L}(\Phi\Phi^\top \rho_{\text{ref}})(\mathbf{x}).$$

As shown in the following proposition, a SoS function remains SoS after integrating over one variable.

Proposition 1 (Integration over one variable). Let \mathcal{L} be the integration operator over the variable x_ℓ with $\ell \in \{1, \dots, d\}$ defined by

$$\mathcal{L}g(\mathbf{x}) = \int_{\mathcal{X}_\ell} g(\mathbf{x}_{-\ell}, x_\ell) dx_\ell.$$

Let g_A be a SoS function as in (15) with $\rho_{\text{ref}}(\mathbf{x}) = \prod_{i=1}^d \rho_{\text{ref}_i}(x_i)$ and $(\Phi(\mathbf{x}))_{\sigma(\alpha)} = \prod_{i=1}^d \phi_{\alpha_i}^i(x_i)$, where $\{\phi_1^\ell, \phi_2^\ell, \dots\}$ are orthonormal functions in $L^2_{\rho_{\text{ref}_\ell}}(\mathcal{X}_\ell)$. Then we have

$$\mathcal{L}g_A(\mathbf{x}) = (\Phi_{-\ell}(\mathbf{x}_{-\ell})^\top A_{-\ell} \Phi_{-\ell}(\mathbf{x}_{-\ell})) \rho_{\text{ref}}(\mathbf{x}_{-\ell}), \quad (24)$$

where $A_{-\ell}$ and $\Phi_{-\ell}(\mathbf{x}_{-\ell})$ are respectively the PSD matrix and the feature map defined as follow. Denote by $\mathcal{K}_{-\ell} = \{\alpha_{-\ell} : \alpha \in \mathcal{K}\}$ the multi-index obtained by removing the ℓ -th components of the elements of \mathcal{K} , and by $\sigma_{-\ell} : \mathcal{K}_{-\ell} \rightarrow \{1, \dots, |\mathcal{K}_{-\ell}|\}$ the lexicographical order for $\mathcal{K}_{-\ell}$. The feature map $\Phi_{-\ell}$ is defined by $(\Phi_{-\ell}(\mathbf{x}_{-\ell}))_{\sigma_{-\ell}(\alpha_{-\ell})} = \prod_{i \neq \ell} \phi_{\alpha_i}^i(x_i)$. The PSD matrix $A_{-\ell}$ is defined by

$$A_{-\ell} = P(A \odot M)P^\top, \quad (25)$$

where \odot denotes the Hadamard product and $P \in \mathbb{R}^{|\mathcal{K}_{-\ell}| \times m}$ and $M \in \mathbb{R}^{m \times m}$ are given by

$$M_{\sigma(\alpha)\sigma(\beta)} = \delta_{\alpha_\ell, \beta_\ell} \quad \text{and} \quad P_{\sigma_{-\ell}(\alpha_{-\ell})\sigma(\beta)} = \prod_{k \neq \ell} \delta_{\alpha_k, \beta_k}, \quad (26)$$

for all $\alpha, \beta \in \mathcal{K}$.

Proof. See Appendix A.1 □

The next corollary, given without proof, shows that Proposition 1 permits to integrate over several variables.

Corollary 1 (Integration over several variables). Proposition 1 can be applied iteratively to integrate over an arbitrary set of variables indexed by $\ell \subset \{1, \dots, d\}$, meaning $\mathcal{L}g_A(\mathbf{x}) = \int g_A(\mathbf{x}_{-\ell}, \mathbf{x}_\ell) d\rho_{\text{ref}_\ell}$, where $\mathbf{x}_\ell = (x_i)_{i \in \ell}$. In particular, the integration over all the variables $\mathcal{L}g_A = \int g_A(\mathbf{x}) d\rho_{\text{ref}}(\mathbf{x})$ is given by

$$\int_{\mathcal{X}} \Phi(\mathbf{x})^\top A \Phi(\mathbf{x}) d\rho_{\text{ref}}(\mathbf{x}) = \text{trace}(A). \quad (27)$$

Remark 3.2. For the fully tensorized set $\mathcal{K} = \mathcal{K}_1 \times \dots \times \mathcal{K}_d$ with $\mathcal{K}_k = \{1, \dots, r_k\}$ the matrices M and P as in (26) are

$$P^\top = I_{r_1} \otimes \dots \otimes I_{r_{\ell-1}} \otimes \mathbf{1}_{r_\ell} \otimes I_{r_{\ell+1}} \otimes \dots \otimes I_{r_d},$$

$$M = \mathbf{1}_{r_1 \times r_1} \otimes \dots \otimes \mathbf{1}_{r_{\ell-1} \times r_{\ell-1}} \otimes I_{r_\ell} \otimes \mathbf{1}_{r_{\ell+1} \times r_{\ell+1}} \otimes \dots \otimes \mathbf{1}_{r_\ell \times r_\ell},$$

where $\mathbf{1}_{r_\ell} \in \mathbb{R}^{r_\ell}$ and $\mathbf{1}_{r_\ell} \in \mathbb{R}^{r_\ell \times r_\ell}$ are respectively the vector and the matrix full with ones and I_r identity matrices of size r .

Remark 3.3 (Non orthonormal basis). If the basis $\{\phi_1^\ell, \phi_2^\ell, \dots\}$ is not orthonormal, then M from Proposition 1 is replaced with

$$M_{\sigma(i)\sigma(j)} = \int_{\mathcal{X}_l} \phi_{i_l}(x_l) \phi_{j_l}(x_l) d\rho_{\text{ref}_l}(x_l).$$

3.3 SoS densities and Knothe-Rosenblatt map

Consider the normalized SoS function, which we refer to as SoS density, defined by

$$\pi_A(\mathbf{x}) = \frac{\Phi(\mathbf{x})^\top A \Phi(\mathbf{x})}{\text{trace}(A)} \rho_{\text{ref}}(\mathbf{x}). \quad (28)$$

By (27), π_A integrates to one and is a well defined probability density function. Next, we show how to compute the Knothe-Rosenblatt (KR) map \mathcal{Q}_A which is the unique triangular map (up to variable ordering) such that $(\mathcal{Q}_A)_\# \rho_{\text{ref}} = \pi_A$, see [36]. Let us factorize π_A as the product of its conditional marginals

$$\pi_A(x) = \pi_A(x_1) \pi_A(x_2|x_1) \dots \pi_A(x_n|x_1, \dots, x_{n-1}), \quad (29)$$

where $\pi_A(x_i|x_1, \dots, x_{i-1})$ is the conditional marginal density given by

$$\pi_A(x_i|x_1, \dots, x_{i-1}) = \frac{\pi_A(x_1, \dots, x_i)}{\pi_A(x_1, \dots, x_{i-1})}, \quad (30)$$

$$\pi_A(x_1, \dots, x_i) = \int \pi_A(x_1, \dots, x_i, x'_{i+1}, \dots, x'_d) dx'_{i+1} \dots dx'_d. \quad (31)$$

We also denote by $\Pi_A(x_i|x_1, \dots, x_{i-1})$ the cumulative distribution function (CDF) of the i -th conditional of π_A , given by

$$\Pi_A(x_i|x_1, \dots, x_{i-1}) = \int_{-\infty}^{x_i} \pi_A(x'_i|x_1, \dots, x_{i-1}) dx'_i. \quad (32)$$

Let $\overline{\mathcal{Q}}_A : [0, 1]^d \rightarrow \mathcal{X}$ be the triangular map defined by recursion as follow

$$\overline{\mathcal{Q}}_A(\xi_1, \dots, \xi_d) = \begin{pmatrix} x_1 \\ x_2 \\ \vdots \\ x_d \end{pmatrix} = \begin{pmatrix} \Pi_A^{-1}(\xi_1) \\ \Pi_A^{-1}(\xi_2|x_1) \\ \vdots \\ \Pi_A^{-1}(\xi_d|x_1, \dots, x_{d-1}) \end{pmatrix}, \quad (33)$$

where $\Pi_A^{-1}(\cdot|x_1, \dots, x_{i-1})$ is the reciprocal function of the monotone function $\Pi_A(\cdot|x_1, \dots, x_{i-1})$. By construction, the map $\overline{\mathcal{Q}}_A$ pushes forward the uniform measure $\mu = \mathcal{U}([0, 1]^d)$ to π_A , meaning $(\overline{\mathcal{Q}}_A)_\# \mu = \pi_A$. Let $\overline{\mathcal{Q}}_0$ be the KR map of ρ_{ref} such that $(\overline{\mathcal{Q}}_0)_\# \mu = \rho_{\text{ref}}$. Finally, we let $\mathcal{Q}_A : \mathcal{X} \mapsto \mathcal{X}$ be the KR map of π_A such that

$$(\mathcal{Q}_A)_\# \rho_{\text{ref}} = \pi_A, \quad \text{where} \quad \mathcal{Q}_A(\mathbf{x}) = \overline{\mathcal{Q}}_A \circ \overline{\mathcal{Q}}_0^{-1}(\mathbf{x}). \quad (34)$$

Hence, we can define the set \mathcal{M} of the variational problem in Eq. (3) as KR maps parametrized with A , given by

$$\mathcal{M}_{\text{SoS}} = \{\mathcal{Q}_A : \mathcal{X} \rightarrow \mathcal{X} \text{ as in (34), where } A \succeq 0\}. \quad (35)$$

The procedure of constructing $\overline{\mathcal{Q}}_A$ (and thus \mathcal{Q}_A) is summarized in Figure 2. By Proposition 1, all the marginals are readily computable and, by using an orthonormal polynomial basis, all the antiderivatives are computable in closed form.

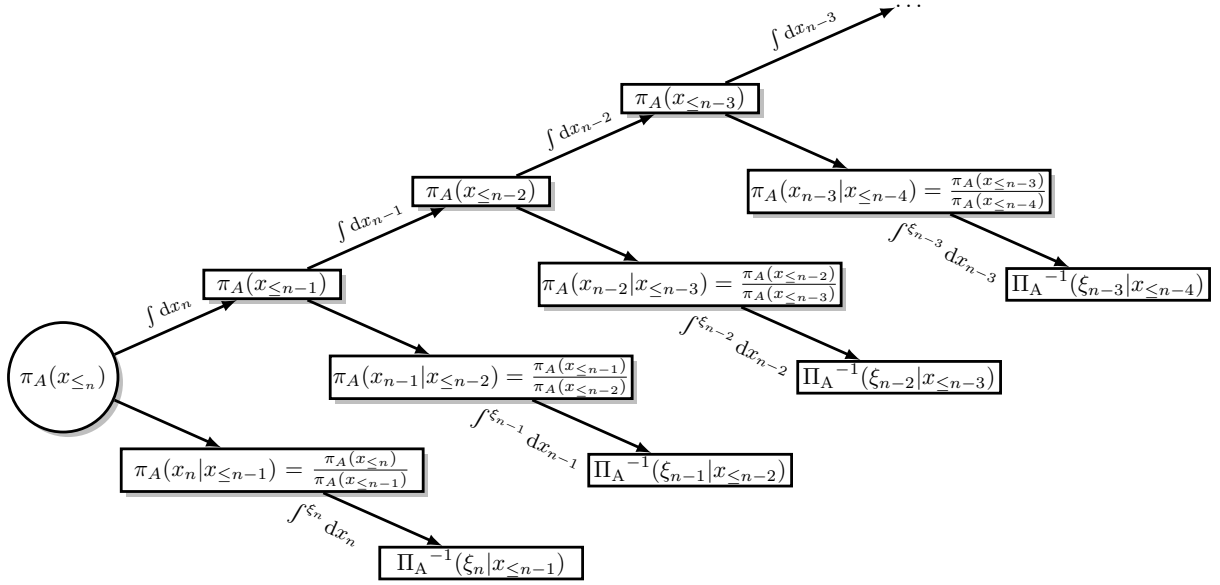


Figure 2: Visualization of the construction of $\bar{\mathcal{Q}}_A$ from a given density π_A . First, one creates the needed marginalization of π_A and the conditionals $\pi_A(x_i|x_1, \dots, x_{n-1}) = \pi(x_i|x_{\leq i-1})$. Then, the CDFs are computed by calculating the antiderivatives, which gives access to the RT. The inverse RT is constructed by inversion of the CDFs according to formula (33).

Remark 3.4 (Identity map). Because ρ_{ref} is a product measure, $\bar{\mathcal{Q}}_0^{-1}(\mathbf{x})$ is a diagonal map with $(\bar{\mathcal{Q}}_0^{-1}(\mathbf{x}))_i = \int_{-\infty}^{x_i} \rho_{\text{ref}_i}(x'_i) dx'_i$ being the CDF of ρ_{ref_i} . In addition, if the basis Φ contains the constant function, meaning $u_0^\top \Phi(\mathbf{x}) = 1$ for some $u_0 \in \mathbb{R}^m$, then $\bar{\mathcal{Q}}_0 = \bar{\mathcal{Q}}_{A_0}$ with $A_0 = u_0 u_0^\top$. Under this condition, the set \mathcal{M} contains the identify map $\bar{\mathcal{Q}}_{A_0} \circ \bar{\mathcal{Q}}_0^{-1} = id$.

Example 3 (Defining ρ_{ref} on indefinite domains). Assume $\text{supp}(\pi) = \mathbb{R}^d$. The mappings from Example 2 can be modified (by an affine change in coordinates from $[-1, 1]$ to $[0, 1]$) to satisfy $(\bar{\mathcal{Q}}_0)_\# \mu = \rho_{\text{ref}}$.

Remark 3.5 (Mapped basis functions on μ). Assume a basis of functions orthonormal in $L^2_\mu([0, 1])$ which are mapped to \mathcal{X} , in the manner of Example 2. Note that, then, $\bar{\mathcal{Q}}_0 = \mathcal{R}$. The map $\bar{\mathcal{Q}}_A$ can be decomposed to $\bar{\mathcal{Q}}_A = \mathcal{R} \circ \tilde{\mathcal{Q}}_A$ where $\tilde{\mathcal{Q}}_A : [0, 1]^d \rightarrow [0, 1]^d$. Furthermore,

$$\mathcal{Q}_A = \mathcal{R} \circ \tilde{\mathcal{Q}}_A \circ \mathcal{R}^{-1}. \quad (36)$$

Applying such maps sequentially allows to save computation by using $\mathcal{R}^{-1} \circ \mathcal{R} = id$.

4 Sequential Transport Map with α -divergence

We build sequential transport maps by using a sequence of bridging densities $\{\pi^{(\ell)}\}_{\ell=1}^L$ so that the sequential maps $\mathcal{T}_\ell = \mathcal{Q}_1 \circ \dots \circ \mathcal{Q}_\ell$ push ρ_{ref} to $\tilde{\pi}^{(\ell)} \approx \pi^{(\ell)}$, with $(\mathcal{T}_\ell)_\# \rho_{\text{ref}} = \tilde{\pi}^{(\ell)}$. \mathcal{T}_ℓ is built recursively as given in Eq. (3).

The classical choice of bridging densities for smooth densities are tempered densities, $\pi^{(\ell)} = \pi^{\beta_\ell}$ with $0 < \beta_1 \leq \dots \leq \beta_L = 1$. For other less widely used bridging methods, we

refer to the literature of sequential Monte Carlo methods [13]. In Section 4.1 we explore the use of bridging densities from diffusion processes when learning from data.

Afterwards, we present two convergence analysis for sequential transport using α -divergences. A previous analysis given in [10] holds solely for the Hellinger distance, a distance for which the triangle inequality holds. Both of our convergence analyses hold for all α -divergences, for which, in general, the triangle inequality does not hold. The determined error bounds by both analyses depend on the distances between two consecutive bridging densities. Let us define a bound for the maximal distance.

Definition 1 (maximal α -divergence between consecutive bridging densities). We define the maximum α -divergence between two consecutive bridging densities by η ,

$$D_\alpha(\pi^{(\ell)} || \pi^{(\ell-1)}) \leq \eta(L) \quad \forall \ell \in [L]. \quad (37)$$

Furthermore, both analyses require that every sequential estimation actually improves upon the previous. We assume this holds.

Assumption 1. We assume there exists $\omega < 1$ such that

$$D_\alpha(\pi^{(\ell)} || \tilde{\pi}^{(\ell)}) \leq \omega D_\alpha(\pi^{(\ell)} || \tilde{\pi}^{(\ell-1)}) \quad \forall \ell \in \{1, \dots, L\}. \quad (38)$$

Remark 4.1 (ω for unnormalized densities). The bound $\tilde{\omega}$ satisfying

$$\sup_{\tilde{\omega}} \left\{ \tilde{\omega} : D_\alpha(f^{(\ell)} || \tilde{f}^{(\ell)}) - Z_{\tilde{f}^{(\ell)}} \phi_\alpha \left(\frac{Z_{f^{(\ell)}}}{Z_{\tilde{f}^{(\ell)}}} \right) \leq \tilde{\omega} D_\alpha(f^{(\ell)} || \tilde{f}^{(\ell-1)}) \right\} \quad (39)$$

bounds ω by

$$\omega \left(\frac{Z_{\tilde{f}^{(\ell+1)}}}{Z_{\tilde{f}^{(\ell)}}} \right)^{\alpha-1} \leq \tilde{\omega}. \quad (40)$$

The first convergence analysis, presented in Section 4.2, uses a quasi triangular inequality for α -divergences, while the second convergence analysis, given in Section 4.3, is more general by utilizing the information geometric properties of α -divergences.

4.1 Bridging densities by diffusion process

We propose a new type of bridging density via the solution of a diffusion process, which are the root of diffusion models in machine learning [39, 40]. In particular, we consider the Ornstein-Uhlenbeck process. For an initial distribution π of the process, the distribution at time $t \geq 0$ is

$$\pi_t(x) = \int \kappa_t(x, y) \pi(y) dy, \quad (41)$$

where

$$\kappa_t(x, y) = \frac{1}{(2\pi(1 - e^{-2t}))^{d/2}} \exp \left(-\frac{\|x - e^{-t}y\|^2}{2(1 - e^{-2t})} \right). \quad (42)$$

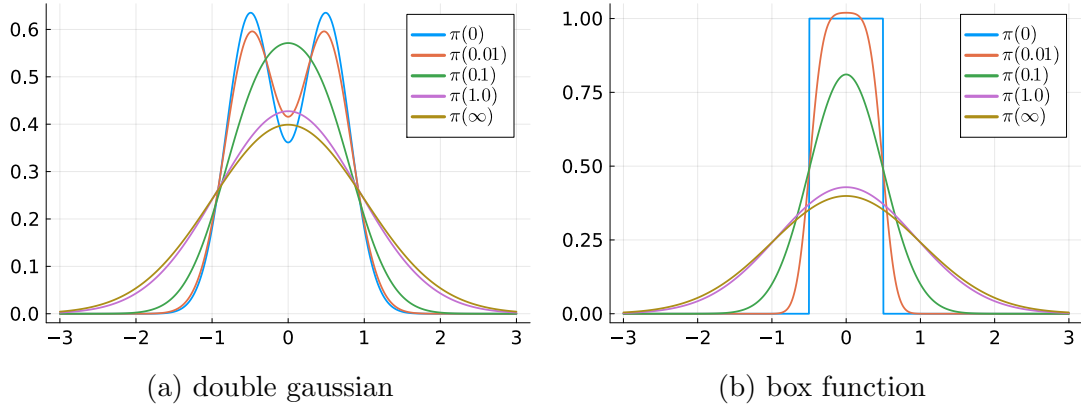


Figure 3: Ornstein-Uhlenbeck process at different time steps for $X(0)$ being distributed according to a double gaussian (a) and a box function (b).

At time $t = 0$, π_t equals π , while for $t \rightarrow \infty$, it approaches to a Gaussian. We then define our bridging densities along the time inverse path of the process, so that

$$\pi^{(\ell)} = \pi_{t_\ell} \quad (43)$$

with $t_1 > t_2 > \dots > t_L = 0$. Hence, this provides us with a path from the reference to the final distribution. Figure 3 visualizes the Ornstein-Uhlenbeck distribution at different times t for two different initial distributions. Evaluating this integral is challenging, especially in cases in which the evaluation of π is computationally expensive. However, this can be avoided when working with samples x from π , $x \sim \pi$, since there exist an SDE in particle form describing the process given by

$$dX(t) = \nabla_X \log \rho(X(t))dt + dW \quad (44)$$

where ρ is a Gaussian. This exact method to create a diffusion path is known in the machine learning community as *Langevin flow* or *Langevin diffusion* [35].

Based on this idea, we propose an algorithm for learning the distribution of a given set of samples. Given $X = \{x_i\}_{i=1}^N$, with $x_i \sim \pi$, we split the set into a training X_{train} and validation set X_{val} , so that $X_{\text{train}} \cup X_{\text{val}} = X$. We estimate a sequence of densities from time evolved samples from X_{train} of the time reverse Langevin diffusion with time steps approaching exponentially to 0 chosen by the function \mathcal{F} (in our case, depending on a given parameter β and the data dimension d). We do this until we begin to overfit, which we determine by crossvalidation using the negative log-likelihood of X_{val} . The algorithm is summarized in Algorithm 1.

We propose a specific time step function \mathcal{F} given by

$$\mathcal{F}(t_{\ell-1}; \beta, d) := -\frac{1}{2} \ln \left(1 - \frac{1 - \exp(-2t_{\ell-1})}{\beta^{2/d}} \right), \quad (45)$$

based on heuristics and the idea that the $\|\pi_t\|_\infty$ is bounded and exponentially decaying with t and some heuristics, which we explain in more details in Appendix C. More generally, any function \mathcal{F} can be used which approaches to 0, optimally, limiting $\omega\beta$, $\omega(1 + \epsilon)$, or η .

Algorithm 1: Sequential transport from data with diffusion process and stopping criterion.

Input: $X_{\text{train}}, X_{\text{val}}, \beta, N$

- 1 $R(\mathcal{T}) = -\sum_{x \in X_{\text{val}}} \log \mathcal{T}_{\#} \rho_{\text{ref}}(x);$
- 2 $\ell = 0;$
- 3 $t_\ell = \infty;$
- 4 $\mathcal{T}_\ell = \text{id};$
- 5 **repeat**
- 6 $\ell \leftarrow \ell + 1;$
- 7 $t_\ell = \mathcal{F}(t_{\ell-1}; \beta, d);$
- 8 $X_\ell = \{x_i^{(\ell)}\}$, where $x_i^{(\ell)} \in X_{\text{train}}$ is one solution of Eq. (44) for time t_ℓ and $X(0) = x_i;$
- 9 $\tilde{\pi}^{(\ell)}(x) = \arg \min_{\tilde{\pi} \in \text{SoS}} -\sum_{x \in X_{\text{train}}} \log \tilde{\pi}^{(\ell)}(x);$
- 10 $\mathcal{T}_\ell = \mathcal{T}_{\ell-1} \circ (\text{Rosenblatt transport of } \tilde{\pi}^{(\ell)}(x));$
- 11 **until** $R(\mathcal{T}_\ell) \leq R(\mathcal{T}_{\ell-1})$ **OR** $\ell > N;$

Output: \mathcal{T}_ℓ

4.2 Convergence analysis using density ratio

In the following, we establish a property of the α -divergences which we can use instead of a triangular inequality in our first convergence analysis.

Proposition 2 (Triangular-like inequalities for probabilities). Let p, ν, q be three probability densities. Furthermore, we assume there exists $\gamma_\alpha^x > 1$ for $x \in \{p, q\}$ so that

$$\sup \left(\frac{x}{\nu} \right)^\alpha \leq \gamma_\alpha^x. \quad (46)$$

Then, for $\alpha \notin \{0, 1\}$, we have

$$D_\alpha(p||q) \leq \gamma_{1-\alpha}^q D_\alpha(p||\nu) + D_\alpha(\nu||q) + \left| \frac{\gamma_{1-\alpha}^q}{\alpha - 1} \right| \quad (47)$$

$$D_\alpha(p||q) \leq D_\alpha(p||\nu) + \gamma_\alpha^p D_\alpha(\nu||q) + \left| \frac{\gamma_\alpha^p}{\alpha} \right|. \quad (48)$$

For the KL-divergence ($\alpha = 1$) we have

$$D_{\text{KL}}(p||q) \leq D_{\text{KL}}(p||\nu) + \gamma_1^p D_{\text{KL}}(\nu||q) \quad (49)$$

and the reverse KL divergence $\alpha = 0$ by duality.

Proof. See Appendix A.4. □

Our analysis only uses the second inequality, hence, we assume a finite bound for γ which holds for all sequential approximations.

Assumption 2. We assume

$$\beta(L) := \sup_{\ell \leq L} \sup_{x \in \mathcal{X}} \left(\frac{\pi^{(\ell+1)}(x)}{\pi^{(\ell)}(x)} \right)^\alpha < +\infty. \quad (50)$$

Based on these definitions and assumptions, we give our first convergence bound in the following proposition.

Proposition 3. Assume Assumptions 1 and 2 hold. Furthermore, let $D_\alpha(\pi^{(0)}||\tilde{\pi}^{(0)}) = 0$, for example by $\pi^{(0)} = \rho_{\text{ref}}$. If $\omega\beta < 1$, then the α -divergence of the estimation of $\pi^{(L)}$ by $\tilde{\pi}^{(L)}$, with $\alpha \neq 0$, converges with

$$D_\alpha(\pi^{(L)}||\tilde{\pi}^{(L)}) \leq \frac{\omega\beta}{1-\omega\beta} \left[\eta(L) + \frac{\beta}{\alpha} \right]. \quad (51)$$

Proof. See Appendix A.5. □

Remark 4.2 (Comparison with bound for Hellinger distance in [10]). In [10], for the same preconditioning procedure an error bound for the Hellinger distance of

$$D_{\text{Hell}}(\pi^{(L)}||\tilde{\pi}^{(L)}) \leq \frac{1}{2} \frac{\sqrt{\omega}}{1-\sqrt{\omega}} \sqrt{\eta(L)} \quad (52)$$

is given, where ω and η are the bounds for $\alpha = 0.5$, the squared Hellinger distance (see Eq. (7)). For the derivation see A.7. The bound we derived here translates for the Hellinger distance to

$$D_{\text{Hell}}(\pi^{(L)}||\tilde{\pi}^{(L)}) \leq \frac{1}{2} \sqrt{\frac{\omega\beta}{1-\omega\beta}} \sqrt{\eta(L) + 2\beta} \quad (53)$$

Remark 4.3 (Bound for KL divergence). For the KL divergence, η can be bounded by $\eta \leq \log(\beta)$ and it holds that

$$D_{\text{KL}}(\pi^{(L)}||\tilde{\pi}^{(L)}) \leq \frac{\omega\beta}{1-\omega\beta} (\log \beta + \beta). \quad (54)$$

4.3 Convergence analysis using α -geodesic

Instead of the triangular like property of α -divergence used in the previous analysis, we use the geometric properties of α -divergences in our second convergence analysis. While we summarize the geometric properties needed for our analysis, for a detailed introduction into the geometry of α -divergences, we refer to [1].

α -divergences give \mathbb{R}_+^n a dually flat structure. In general, this is not the case for the space of probability distributions, except for the KL and reverse KL-divergence, see [1, p. 74]. Hence, in the following, we always work in \mathbb{R}_+^n . Let us state the definition of the (dual) α -geodesic.

Definition 2 (α and α^* -geodesic [1]). The α -geodesic connecting two unnormalized densities p and q is given by

$$\mu_t(x) = \begin{cases} \{(1-t)p(x)^{1-\alpha} + tq(x)^{1-\alpha}\}^{\frac{1}{1-\alpha}} & \text{for } \alpha \neq 1 \\ p(x)^{1-t}q(x)^t & \text{for } \alpha = 1 \end{cases}$$

Furthermore, the $(1-\alpha)$ -geodesic is the α^* -geodesic (dual α -geodesic).

In our analysis, we make use of the projection theorem and generalized Pythagorean theorem, which we state in the following.

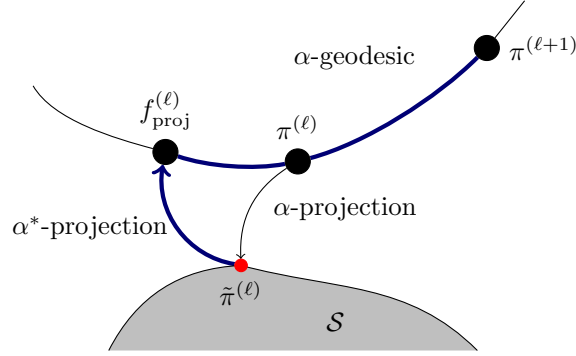


Figure 4: Visualization of the α -geodesic going through $\pi^{(\ell)}$ and $\pi^{(\ell+1)}$ as well as the approximation submanifold \mathcal{S} with the approximation $\tilde{\pi}^{(\ell)}$ being the α -projection of $\pi^{(\ell)}$ onto \mathcal{S} . The α^* -projection back on the α -geodesic is used in order to use the generalized Pythagorean theorem between $\tilde{\pi}^{(\ell)}$, $f_{\text{proj}}^{(\ell)}$, and $\pi^{(\ell+1)}$.

Theorem 4.4 (generalized Pythagorean theorem [1]). Given three measures, f, g, h , so that the α -geodesic between f and g and the α^* -geodesic between g and h is orthogonal. Then,

$$D_\alpha(f||h) = D_\alpha(f||g) + D_\alpha(g||h). \quad (55)$$

Theorem 4.5 (Projection theorem [1]). Consider a measure g and a submanifold \mathcal{S} .

$$\min_{\tilde{g} \in \mathcal{M}} D_\alpha(g||\tilde{g}) \quad (56)$$

is an α -projection onto \mathcal{M} . The minimizer is unique if \mathcal{M} is an α^* -flat submanifold (sometimes referred to as α^* -convex set).

Let us define an α -geodesic μ_t which connects two consecutive bridging densities $\pi^{(\ell)}$ and $\pi^{(\ell+1)}$, as shown in Figure 4. An approximation of $\pi^{(\ell)}$ by $\tilde{\pi}^{(\ell)}$ is found by minimizing the variational density estimation problem, which in the geometric interpretation is a projection from $\pi^{(\ell)}$ onto the approximation manifold \mathcal{S} , following an α -geodesic. From an information geometric view, this has a unique solution, if \mathcal{S} is an α^* -flat submanifold of \mathbb{R}_+^n , which means, that all geodesics connecting two points in \mathcal{S} are contained in \mathcal{S} . In our work, this is not necessarily the case and not further necessary for this convergence analysis.

Next, we project the approximation $\tilde{\pi}^{(\ell)}$ back onto a point $f_{\text{proj}}^{(\ell)}$ on the α -geodesic between $\pi^{(\ell)}$ and $\pi^{(\ell+1)}$. This projection is defined by

$$f_{\text{proj}}^{(\ell)} = \arg \min_{\mu_t \in \alpha\text{-geodesic}} D_\alpha(\mu_t || \tilde{\pi}^{(\ell)}) \quad (57)$$

and follows the α^* -geodesic between these points. Furthermore, $f_{\text{proj}}^{(\ell)}$ is unique, since, by definition, the α^* -geodesic is α^* -flat. For an visualization of these projections, see Fig. 4.

This allows us to use the generalized Pythagorean theorem between $\tilde{\pi}^{(\ell)}$, $f_{\text{proj}}^{(\ell)}$, and $\pi^{(\ell+1)}$. In the following, we make an assumption about the distance between $f_{\text{proj}}^{(\ell)}$ and $\pi^{(\ell)}$.

Assumption 3. We assume that there exists an $\epsilon \geq 0$ so that

$$D_\alpha(\pi^{(\ell+1)} || f_{\text{proj}}^{(\ell)}) \leq (1 + \epsilon) D_\alpha(\pi^{(\ell+1)} || \pi^{(\ell)}) \quad \forall l \in [L]. \quad (58)$$

Based on these two assumptions, we can establish a convergence bound for α -divergences.

Proposition 4 (Self-reinforced error bound for α -divergences). Let assumptions 1 and 3 be true. Furthermore, let $D_\alpha(\pi^{(0)}||\tilde{\pi}^{(0)}) = 0$, for example by $\pi^{(0)} = \rho_{\text{ref}}$. If $\omega < 1$, then the estimation of $\pi^{(L)}$ is bounded with

$$D_\alpha(\pi^{(L)}||\tilde{\pi}^{(L)}) \leq \frac{\omega(1+\epsilon)}{1-\omega}\eta(L). \quad (59)$$

Proof. See Appendix A.6. □

Remark 4.6 (Hellinger distance). The Hellinger distance is symmetric. Since the α^* -geodesic is (by definition) an α^* -flat manifold, the α -projection to f_{proj}^ℓ is unique. Following, that for the Hellinger distance the α -geodesic and α^* -geodesic are equivalent, $\pi^{(\ell)} = f_{\text{proj}}^{(\ell)}$ if $\tilde{\pi}^{(\ell)}$ is unique (that is, if \mathcal{S} is an α -flat submanifold). This is for example the case for squared functions, so that a probability density $\pi \propto p^2$ which are used in [10, 44, 11], but not for SoS functions. For squared function $\epsilon = 0$ and the bound we derive is

$$D_{\text{Hell}}(\pi^{(L)}||\tilde{\pi}^{(L)}) \leq \frac{1}{2}\sqrt{\frac{\omega}{1-\omega}}\sqrt{\eta(L)}. \quad (60)$$

Notice that this error bound is strictly better compared to the bound in [10] given in Eq. (52), which we show Appendix A.7.

5 Density estimation in high dimensions

The SoS densities presented do not scale well in high dimension due to the exponential increase of $|\mathcal{K}|$ with respect to d , see (23). In the following, we summarize two methods which can be used to scale to higher dimensions.

5.1 Subspace projection: the lazy maps

One strategy is to iteratively select a subspace of \mathcal{X} in which to perform density estimation. In the following, let $\mathcal{X} = \mathbb{R}^d$. A low dimensional map on a linear subspace $U \in \mathbb{R}^{d \times r}$, where $r \ll d$ is the reduced dimension, writes

$$\mathcal{Q}_\ell(\mathbf{x}) = U_\ell \tilde{\mathcal{Q}}_\ell(U_\ell^\top \mathbf{x}) + (1 - U_\ell U_\ell^\top) \mathbf{x} \quad (61)$$

where $\tilde{\mathcal{Q}} : \mathbb{R}^r \rightarrow \mathbb{R}^r$ is a low-dimensional map acting on \mathbb{R}^r with $r \ll d$. By iteratively working on different subspaces, density estimation can be performed in high dimensions.

This strategy, in the case of working with evaluations of the unnormalized densities, was used in [4] by choosing the subspace by minimizing an upper bound of the KL-divergence. For working with samples out of a distribution, a more sophisticated version was proposed in [2], where score ratio matching is used to find a subspace.

In our work, we use randomly chosen subspaces and let an exploration of other methods open for future work.

5.2 Knowing the conditional independence structure

Consider a given conditional independence structure by an undirected graph $G(V, E)$. For an introduction to such graphical models, we refer to [23]. In this graph, V are the vertices, describing random variables, and E edges, describing dependencies between variables. The conditional independence in this graph is given as follows; Given two vertices which are not *adjacent* $a, b \in G$, so that $\{a, b\} \notin E$, then a and b are conditional independent given all other variables, written as

$$a \perp\!\!\!\perp b | V/\{a, b\} \Leftrightarrow \pi(a, b | V/\{a, b\}) = \pi(a | V/\{a, b\})\pi(b | V/\{a, b\}). \quad (62)$$

The properties of such a model allows to factorize a probability density π according to G . Given a factorization of G by the set of cliques C , there exist non-negative functions (also called couplings) $\phi_c(\mathbf{x})$ for $c \in C$ which only act on a subset of \mathbf{x} , \mathbf{x}_c . Hence, π has the form

$$\pi(\mathbf{x}) = \prod_{c \in C} \phi_c(\mathbf{x}) \quad (63)$$

where ϕ_c are not unique. It is known that this property can be used to reduce the complexity of density estimation and that a sequential composition of lower dimensional maps can be learned to estimate π , as explored in detail in [41].

We provide a conceptual example in Fig. 5 of how to do this, while we refer to [41] for the full explanation. The graphical model we consider consists of 4 variables, where the density can be learned using two sequential maps. We define a first map by

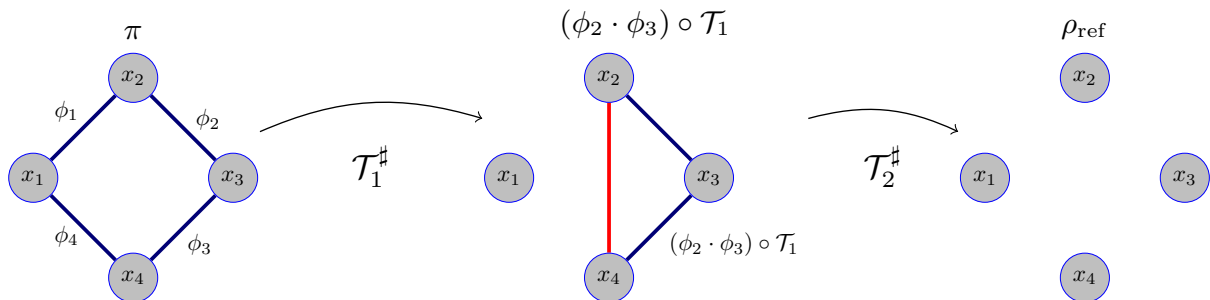


Figure 5: Example of learning a graphical model with 4 variables using 2 sequential maps. A first map only acts on x_1, x_2 , and x_4 and removes any coupling to x_1 while introducing a new coupling between x_2 and x_4 . In a second map, the remaining couplings are removed to end up with the uncorrelated variables distributed according to ρ_{ref} (ρ_{ref} is a product measure).

$$\mathcal{T}_1^\#(\phi_1 \cdot \phi_4)(\mathbf{x}) \propto \rho_{\text{ref}}(\mathbf{x}), \quad (64)$$

where for our example we assume $\rho_{\text{ref}}(x) = \mathcal{U}(x)$, so that $\pi(x)\rho_{\text{ref}}(x) \propto \pi(x)$. It is required that the map \mathcal{T}_1 in its second and fourth variable do not depend on the first, for example

$$\mathcal{T}_1(\mathbf{x}) = \begin{pmatrix} \mathcal{T}_{1,1}(x_1, x_2, x_4) \\ \mathcal{T}_{1,2}(x_2, x_4) \\ x_3 \\ \mathcal{T}_{1,4}(x_4) \end{pmatrix}, \quad (65)$$

so that all other variables in $\mathcal{T}_1^\# \pi$ are independent of x_1 (depicted in the middle Figure of Fig. 5). Consecutively, a second map satisfying

$$\mathcal{T}_2^\# (\phi_2 \cdot \phi_3) (\mathcal{T}_1(\mathbf{x})) \propto \rho_{\text{ref}}(\mathbf{x}) \quad (66)$$

is enough to learn π ,

$$(\mathcal{T}_2 \circ \mathcal{T}_1)^\# \pi(\mathbf{x}) \propto \mathcal{T}_2^\# (\phi_2 \cdot \phi_3) (\mathcal{T}_1(\mathbf{x})) \propto \rho_{\text{ref}}. \quad (67)$$

However, this is based on the assumption that the maps are exact. Let us consider

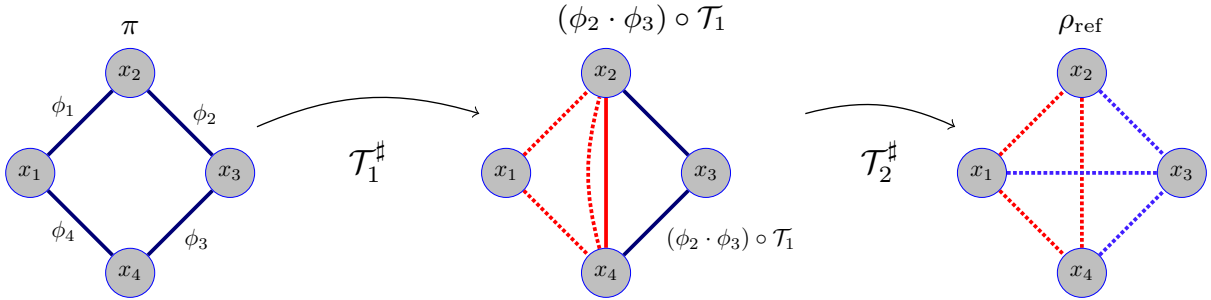


Figure 6: Fig. 5 with assuming an imperfect map \mathcal{T}_1 which creates an error with a dependency shown in dotted red. Consecutively, a general \mathcal{T}_2 spreads this error to more variables, shown in dotted blue.

imperfections, where \mathcal{T}_1 creates an error ϵ_1 which depends on the variables it acts on, $\mathcal{T}_1^\# (\phi_1 \cdot \phi_4) (\mathbf{x}) \propto \epsilon_1(x_1, x_2, x_4)$. Further applying \mathcal{T}_2 , even if this is an exact map, spreads the error ϵ_1 , so that $\mathcal{T}_2^\# \epsilon_1$ depend on all variables in the network. This is depicted in Fig. 6. Hence, when considering imperfect maps, the estimation error does not follow the conditional independence structure of the original model.

6 Numerical Examples

We demonstrate the method presented in this paper with numerical examples, implemented in Julia. Our implementations can be found at <https://github.com/benjione/SequentialMeasureTransport.jl>. For the optimization, we use the *JuMP.jl* library [24] together with *Hypatia.jl*, as an interior point solver [6]. For more details regarding the implementation, see Appendix D.

6.1 Multimodal density from data by diffusion process

We demonstrate the diffusion process given in Section 4.1 by estimating a two modal density, given by

$$\pi_X(\mathbf{x}) \quad \text{with } \mathbf{x} \sim \begin{cases} \mathcal{N} \left(\begin{pmatrix} 2 & 2 \end{pmatrix}^\top, \text{diag} \begin{pmatrix} 0.1 & 0.5 \end{pmatrix} \right) & \text{with probability } 0.5 \\ \mathcal{N} \left(\begin{pmatrix} -2 & -2 \end{pmatrix}^\top, \text{diag} \begin{pmatrix} 0.5 & 0.1 \end{pmatrix} \right) & \text{else.} \end{cases}$$

The density is learned from 1000 independent samples. For the diffusion process, we choose 20 bridging densities with timesteps between $t_1 \approx 1.0 \leq \dots \leq t_{20} = 0.0$. The SoS

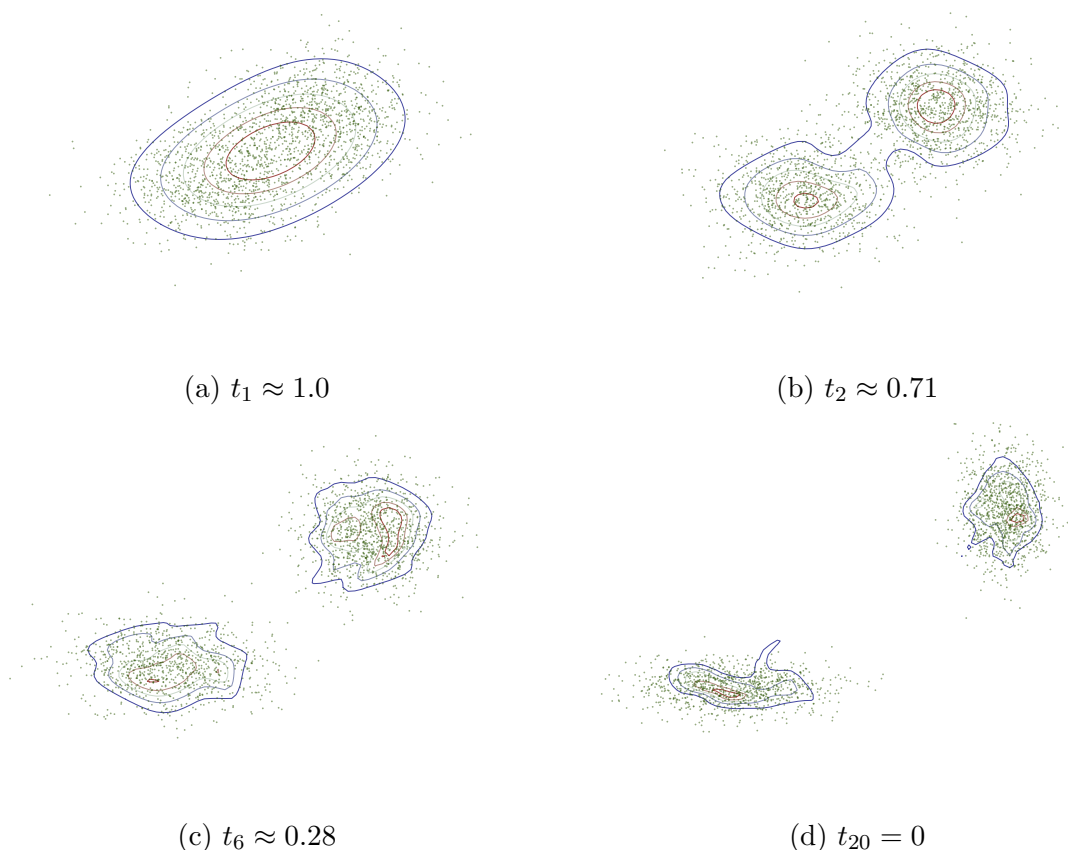


Figure 7: Visualization of the reverse diffusion process at 4 different time steps, where the samples evolved after the given times are visualized as green dots and the estimated density as a contour.

functions we employ for estimating the densities use Legendre polynomials up to order 4. In Fig. 7, we provide a little cartoon of diffused samples and its density estimation at different timesteps in the process. In the first timestep, the distribution is simple enough that our model is able to capture it well. Following the reverse process, the previous estimations are used as preconditioners in order to learn the more and more complicated densities in the reverse diffusion process.

6.2 Density from datasets

We estimate the density of UCI datasets and follow approaches from [3] and [42]. We remove all discrete coefficients and coefficients with Pearson correlation higher than 0.98. We then randomly split the data into a training and test dataset, where 90 % are for training and 10 % for testing and evaluate the negative log likelihood function of the test dataset to evaluate how well the density fits the data. We do this a total of 10 times with different splits in train and test data for a better comparison. This setup is identical with the one in [3] and we compare the results of the negative log likelihood directly. These results are for the adaptive transport map (ATM) algorithm [3] and a multivariate Gaussian estimation.

ATM estimates densities using approximations of the type $g(f(\mathbf{x}))$, where $g : \mathcal{X} \rightarrow \mathbb{R}_+$ and f being a linear function space (polynomials), with an adaptive amount of coefficients

using downward closed sets. Finally, a KR map is build from the approximation.

For our method, we use Algorithm 1 with $\beta = 2.0$ and apply density estimations to randomly picked 8-dimensional subspaces, in order to reduce computation time. For each of this subspaces, we choose polynomials of up to order 3 so that $A \in \mathbb{R}^{70 \times 70}$. The

Table 1: Comparison of log likelihood function for different UCI datasets and density estimation methods. The best results are highlighted in bold.

Dataset	(d, N)	SoS	Gaussian	SoS [s]	ATM	# layers SoS
White wine	(11, 4898)	11.1 ± 0.2	13.2 ± 0.5	1613 ± 250	11.0 ± 0.2	16.4 ± 3.0
Red wine	(11, 1599)	10.0 ± 0.5	13.2 ± 0.3	353 ± 64	9.8 ± 0.4	12.5 ± 2.8
Parkinsons	(15, 5875)	4.4 ± 0.4	10.8 ± 0.4	4022 ± 333	2.8 ± 0.4	29.0 ± 2.7
Boston	(10, 506)	-4.1 ± 1.6	11.3 ± 0.5	646 ± 81.5	3.1 ± 0.6	28.5 ± 4.7

results are depicted in Table 1. For the red and white wine dataset SoS and ATM perform similarly, while for Parkinsons ATM performs significantly better and for Boston SoS performs significantly better. We explain the worse result on Parkinsons with using random subspaces and the higher dimension of this dataset. From the lower dimensional Boston dataset we conclude that our methodology works well in general. We want to mention that Algorithm 1 can also be employed with the adaptive functions from ATM and we believe that this would outperform the SoS, since these scale better to higher dimensions. Our results should only be considered as a proof of concept for the applicability of SoS and diffusion bridging densities, while further work to mitigate the curse of dimensionality is needed.

6.3 Susceptible-Infected-Removed (SIR) model

We consider an example from epidemiology and follow the setting in [11]. Having access to the SIR model, a model describing the spread of a disease, see [20], we want to calibrate parameters of the model given observations on the amount of infected persons at different points in time. The SIR model is given by

$$\begin{aligned}\dot{S}_k &= -\beta_k I_k S_k + \frac{1}{2} \sum_{j \in \mathcal{I}_k} (S_j - S_k) \\ \dot{I}_k &= \beta_k S_k I_k - \gamma_k I_k + \frac{1}{2} \sum_{j \in \mathcal{I}_k} (I_j - I_k) \\ \dot{R}_k &= \gamma_k I_k + \frac{1}{2} \sum_{j \in \mathcal{I}_k} (R_j - R_k)\end{aligned}$$

where $k \in \mathcal{K}$ describes the amount of compartments in the model. In the following, we will only consider $|\mathcal{K}| = 1$. The parameters to be determined are γ_k and β_k . The ODE is simulated for $t \in [0, 5]$ with 6 equidistant observations $y_{k,j}$ in I_k perturbed with noise $\epsilon_{k,j} \sim \mathcal{N}(0, 1)$, so that $y_{k,j} = I_k(t_j) + \epsilon_{k,j}$. We pose the calibration problem in an Bayesian setting, where the prior belief on the parameters is uniform in $[0, 2]$ for all parameters and the likelihood function is gaussian and given by

$$\mathcal{L}(x|y) \propto \exp\left(\frac{-\sum_{k=1, j=1}^{K, 6} (I_k(\frac{5j}{6}; x) - y_{k,j})^2}{2}\right)$$

We approximate the posterior using 4 self-reinforced layers with downward closed tensorized polynomials in Φ of maximum degree 6. We choose bridging densities of type $\pi^{(l)} = \pi_{\text{post}}(x)^{\beta_l}$ with $\beta_1 = 1/8$, $\beta_2 = 1/4$, $\beta_3 = 1/2$ and $\beta_4 = 1$ and use 1000 evaluations of the unnormalized posterior for each layer. A comparison between the contours of the

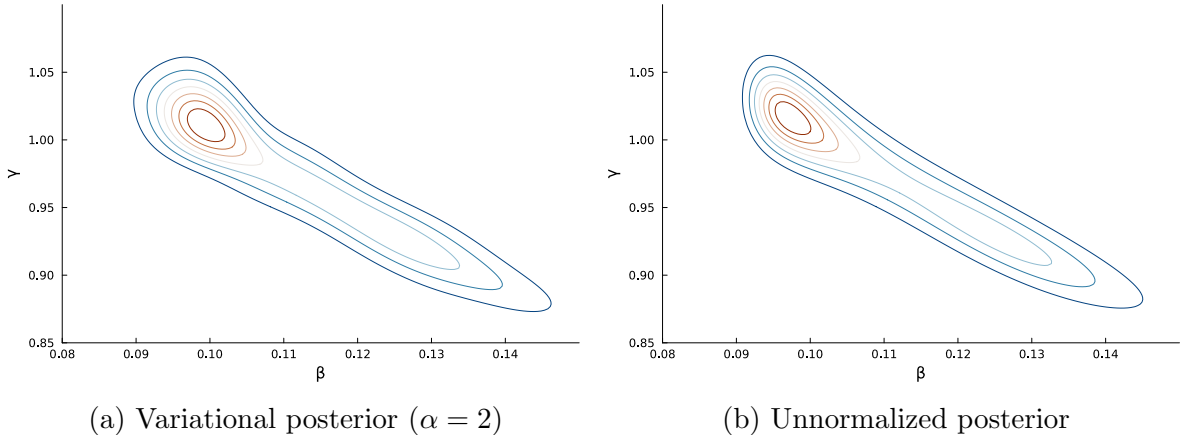


Figure 8: Comparison of the variational density (a) and the unnormalized posterior distribution (b) for the parameter space around the center of mass, for $\gamma \in [0.85, 1.1]$ and $\beta \in [0.08, 0.15]$.

variational posterior and unnormalized posterior around the center of mass is depicted in Fig. 8. Visually, the density estimation fits the true density well. To quantify our results, we consider the estimated density for the task of self-normalized importance sampling and calculate the *effective sampling size* (ESS). To do this, we run the density estimation 10 times with drawing new noise $\epsilon_{k,j}$ in every iteration and calculate the ESS for density estimation using α -divergences between 0.4 and 3.0. The results are shown in Figure 9. As expected, for higher α a better ESS is achieved. This is because the ESS can be

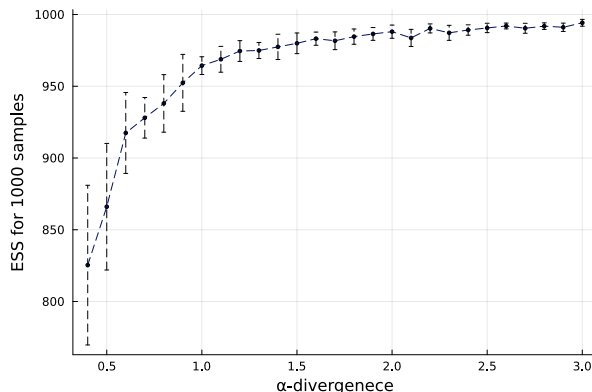


Figure 9: ESS for α -divergence between $\alpha = 0.4$ and $\alpha = 3.0$ for 10 runs on the SIR model with different realizations of noise. The ESS is given as effective samples for 1000 samples.

written as $\text{ESS} = 1/(1 + \text{Var}_{\tilde{\pi}}[Z_f])$ and minimizing the χ^2 -divergence is equivalent to minimizing $\text{Var}_{\tilde{\pi}}[Z_f]$ (e.g. see [27]). Since higher α -divergences are upper bounds on the χ^2 -divergence, it is expected that minimizing over them performs similarly. Furthermore, because of the zero avoiding property for $\alpha \geq 1$, which is a requirement for successful

importance sampling in a lot of cases, higher α for estimations of densities for importance sampling is desirable.

6.4 Gaussian graphical model

We give a demonstration of estimating graphical models using a sequence of maps. For simplicity, we use a Gaussian graphical model, in which the distributions remains Gaussian. We use the conditional independence structure from Fig. 5 where the total distribution, $\pi \propto \phi_1\phi_2\phi_3\phi_4$ is a normal distribution with expectation and covariance given by

$$\mu = \begin{pmatrix} 0 \\ 0 \\ 0 \\ 0 \end{pmatrix} \quad \text{and} \quad \Sigma = \begin{pmatrix} 0.26 & 0.2 & 0.16 & -0.12 \\ 0.2 & 0.24 & 0.19 & -0.14 \\ 0.16 & 0.19 & 0.24 & -0.18 \\ -0.12 & -0.14 & -0.18 & 0.29 \end{pmatrix}. \quad (68)$$

We perform tempering, by first tempering on $\phi_1 \cdot \phi_4$ using 4 layers. Afterwards, we learn the density $\phi_2 \cdot \phi_3$, also using tempering with 4 layers. To demonstrate our result, we compare samples of the marginal distribution $\pi(x_1, x_3)$ with the density function of the true marginal, given in Fig. 10.

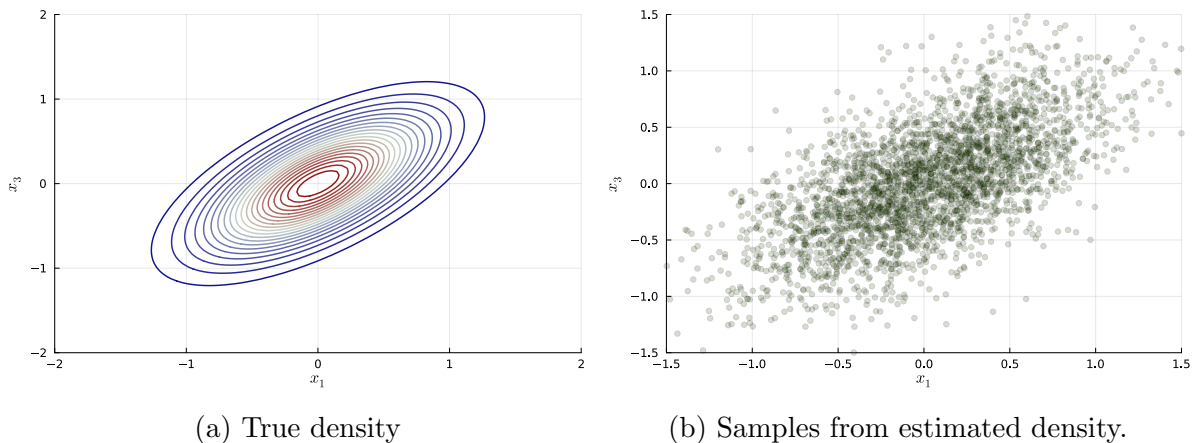


Figure 10: Comparison of marginal density $\pi(x_1, x_3)$ in (a) with samples from the estimated density (b).

7 Conclusion and Outlook

We introduced SoS functions for density approximation utilizable with a wide range of statistical divergences. We embedded this tool into the framework of measure transport [26] and used it in the context of sequential transport, as in [10]. The SoS functions we proposed are a generalization of [11] and [44] with an extension to general divergences. To the best of our knowledge, our work is the first in measure transport to propose a linear function space in \mathbb{R}_+^n to be utilizable with any convex statistical divergence.

We provided two convergence analysis for greedy density estimation, a first with intuitive assumptions and a second one which allowed us to improve the bound for the

Hellinger distance in [10]. We demonstrated the applicability of our method with numerical examples. In order to make our proposed method better applicable, future work is necessary, from which in our opinion the most important ones are:

- **Sampling**

While optimal sampling is well established for least squares in linear approximation spaces, we do not know how to do this for SoS functions.

- **Approximation rates**

Since SoS functions generalize squared polynomials, results from [44] are applicable, but a work on more general approximation rates for SoS functions is missing.

- **Bridging densities**

The bridging densities obtained by tempering work well for continuous distributions and the diffusion when working with samples out of π . However, we believe that bridging densities for discontinuous distributions and with guarantees of convergence are missing.

- **High dimensionality**

Our method does not scale well with high dimensions. In our numerical example, in Sec. 6, we used random subspaces to deal with the higher dimensions. We think that our method can be transformed into a tensor version to make it scale better with high dimensions.

A Proofs

A.1 Proof of Proposition 1

This proof is inspired by [11] where the marginalization is done for squared polynomials only. We can write

$$\begin{aligned}
\mathcal{L}g_A(\mathbf{x}) &= \int \Phi(\mathbf{x}_{-\ell}, x'_\ell)^\top A \Phi(\mathbf{x}_{-\ell}, x'_\ell) d\mu_\ell(x'_\ell) \\
&= \sum_{\alpha, \beta \in \mathcal{K}} A_{\sigma(\alpha)\sigma(\beta)} \left(\prod_{i \neq \ell} \phi_{\alpha_i}^i(x_i) \right) \left(\prod_{i \neq \ell} \phi_{\beta_i}^i(x_i) \right) \int \phi_{\alpha_\ell}(x'_\ell) \phi_{\beta_\ell}(x'_\ell) d\mu_\ell(x'_\ell) \\
&= \sum_{\alpha, \beta \in \mathcal{K}} \hat{\Phi}_{\sigma(\beta)} A_{\sigma(\alpha)\sigma(\beta)} M_{\sigma(\alpha)\sigma(\beta)} \hat{\Phi}_{\sigma(\alpha)} \\
&= \hat{\Phi}(\mathbf{x}_{-\ell})^\top (A \odot M) \hat{\Phi}(\mathbf{x}_{-\ell})
\end{aligned}$$

where

$$M_{\sigma(\alpha)\sigma(\beta)} = \int \phi_{\alpha_\ell}(x'_\ell) \phi_{\beta_\ell}(x'_\ell) d\mu_\ell(x'_\ell),$$

and $\hat{\Phi}_{\sigma(\alpha)}(\mathbf{x}_{-\ell}) = \prod_{i \neq \ell} \phi_{\alpha_i}^i(x_i)$. Note that the vector $\hat{\Phi}(\mathbf{x}_{-\ell})$ has size $m = |\mathcal{K}|$ and contains duplicated entries of the vector $\Phi_{-\ell}(\mathbf{x}_{-\ell})$ defined by $\hat{\Phi}_{\sigma(\alpha)}(\mathbf{x}_{-\ell}) = \prod_{i \neq \ell} \phi_{\alpha_i}^i(x_i)$. By definition (26) of the matrix $P \in \mathbb{R}^{|\mathcal{K}-\ell| \times m}$, we have $\hat{\Phi}_{\sigma(\alpha)}(\mathbf{x}_{-\ell}) = P^\top \Phi_{-\ell}(\mathbf{x}_{-\ell})$. This shows $M^{-\ell} = P(A \odot M)P^\top$ and concludes the proof.

A.2 Proof of pushforward and pullback in α -divergence

We have

$$D_\alpha(T\#p||q) = \int \phi_\alpha\left(\frac{p \circ T^{-1} \cdot \nabla_x T^{-1}}{q}\right) dq \quad (69)$$

$$= \int \phi_\alpha\left(\frac{p \circ T^{-1} \circ T \cdot \nabla_x T^{-1} \circ T}{q \circ T}\right) dT\#q \quad (70)$$

$$= \int \phi_\alpha\left(\frac{p}{q \circ T \cdot \nabla_x T}\right) dT\#q \quad (71)$$

$$= D_\alpha(p||T\#q) \quad (72)$$

Trivially, this does not only hold for probability distributions but also measures.

A.3 Proof of relation between measures and probabilities in α -divergence

$$D_\alpha(f||g) = \int \phi_\alpha\left(\frac{f}{g}\right) dg \quad (73)$$

$$= \int \frac{Z_f^\alpha \left(\frac{\pi_f}{\pi_g}\right)^\alpha - \left(\frac{Z_f}{Z_g}\right)^\alpha - 1 + 1}{\alpha(\alpha - 1)} Z_g d\pi_g + \int \frac{Z_f \frac{\pi_f}{\pi_g} - \frac{Z_f}{Z_g} - 1 + 1}{\alpha - 1} Z_g d\pi_g \quad (74)$$

$$= \frac{Z_f^\alpha}{Z_g^{\alpha-1}} D_\alpha(\pi_f||\pi_g) + Z_g \left(\frac{\frac{Z_f^\alpha}{Z_g^\alpha} - 1}{\alpha(\alpha - 1)} + \frac{Z_f - 1}{\alpha - 1} \right) \quad (75)$$

$$= \frac{Z_f^\alpha}{Z_g^{\alpha-1}} D_\alpha(\pi_f||\pi_g) + Z_g \phi_\alpha\left(\frac{Z_f}{Z_g}\right). \quad (76)$$

A.4 Proof of Proposition 2

For the inequalities:

We work with probability densities.

Let

$$\tilde{\phi}_\alpha(t) = \frac{t^\alpha - 1}{\alpha(\alpha - 1)} \quad (77)$$

For probabilities, we have

$$D_\alpha(p||q) = \int \phi_\alpha\left(\frac{p}{q}\right) dq = \int \tilde{\phi}_\alpha\left(\frac{p}{q}\right) dq. \quad (78)$$

Note that $\phi_\alpha(t) \geq 0$ for $t > 0$ while this is not the case for $\tilde{\phi}_\alpha$. We assume there exists a $\gamma_\alpha^x > 0$

$$\sup \left(\frac{x}{\nu}\right)^\alpha \leq \gamma_\alpha^x \quad (79)$$

for $x \in \{p, q\}$. For $\alpha \notin \{0, 1\}$

$$\phi_\alpha \left(\frac{p}{q} \right) \stackrel{\nu \geq 0}{=} \frac{\left(\frac{p}{\nu} \right)^\alpha \left(\frac{\nu}{q} \right)^\alpha - 1}{\alpha(\alpha - 1)} - \frac{\frac{p}{q} - 1}{\alpha - 1} \quad (80)$$

$$= \left(\frac{\nu}{q} \right)^\alpha \frac{\left(\frac{p}{\nu} \right)^\alpha - 1}{\alpha(\alpha - 1)} + \frac{\left(\frac{\nu}{q} \right)^\alpha - 1}{\alpha(\alpha - 1)} \pm \left(\frac{\nu}{q} \right)^\alpha \frac{\frac{p}{\nu} - 1}{\alpha - 1} - \frac{\frac{p}{q} - 1}{\alpha - 1} \quad (81)$$

$$= \left(\frac{\nu}{q} \right)^\alpha \phi_\alpha \left(\frac{p}{\nu} \right) + \tilde{\phi}_\alpha \left(\frac{\nu}{q} \right) + \left(\frac{\nu}{q} \right)^\alpha \frac{\frac{p}{\nu} - 1}{\alpha - 1} - \frac{\frac{p}{q} - 1}{\alpha - 1}. \quad (82)$$

Going to the D_α we get

$$D_\alpha(p||q) = \int \left(\frac{\nu}{q} \right)^\alpha \phi_\alpha \left(\frac{p}{\nu} \right) + \tilde{\phi}_\alpha \left(\frac{\nu}{q} \right) + \left(\frac{\nu}{q} \right)^\alpha \frac{\frac{p}{\nu} - 1}{\alpha - 1} - \frac{\frac{p}{q} - 1}{\alpha - 1} d\nu \quad (83)$$

$$\leq \sup \left(\frac{\nu}{q} \right)^{\alpha-1} D_\alpha(p||\nu) + D_\alpha(\nu||q) + \int \left(\frac{\nu}{q} \right)^{\alpha-1} \frac{\frac{p}{\nu} - 1}{\alpha - 1} d\nu \quad (84)$$

For $\alpha > 1$:

$$\leq \sup \left(\frac{\nu}{q} \right)^{\alpha-1} D_\alpha(p||\nu) + D_\alpha(\nu||q) + \frac{\sup \left(\frac{\nu}{q} \right)^{\alpha-1} - \inf \left(\frac{\nu}{q} \right)^{\alpha-1}}{\alpha - 1} \quad (85)$$

$$\leq \gamma_{1-\alpha}^q D_\alpha(p||\nu) + D_\alpha(\nu||q) + \frac{\gamma_{1-\alpha}^q - \inf \left(\frac{\nu}{q} \right)^{\alpha-1}}{\alpha - 1} \quad (86)$$

$$\leq \gamma_{1-\alpha}^q D_\alpha(p||\nu) + D_\alpha(\nu||q) + \frac{\gamma_{1-\alpha}^q}{\alpha - 1} \quad (87)$$

For $\alpha < 1$:

$$\leq \sup \left(\frac{\nu}{q} \right)^{\alpha-1} D_\alpha(p||\nu) + D_\alpha(\nu||q) + \frac{\inf \left(\frac{\nu}{q} \right)^{\alpha-1} - \sup \left(\frac{\nu}{q} \right)^{\alpha-1}}{\alpha - 1} \quad (88)$$

$$\leq \gamma_{1-\alpha}^q D_\alpha(p||\nu) + D_\alpha(\nu||q) + \left| \frac{\gamma_{1-\alpha}^q - \inf \left(\frac{\nu}{q} \right)^{\alpha-1}}{\alpha - 1} \right| \quad (89)$$

$$\leq \gamma_{1-\alpha}^q D_\alpha(p||\nu) + D_\alpha(\nu||q) + \left| \frac{\gamma_{1-\alpha}^q}{\alpha - 1} \right| \quad (90)$$

By duality and $\alpha > 0$ (hence, $1 - \alpha < 1$)

$$D_\alpha(p||q) = D_{1-\alpha}(q||p) \quad (91)$$

$$\leq \gamma_\alpha^p D_{1-\alpha}(q||\nu) + D_{1-\alpha}(\nu||p) + \frac{\gamma_\alpha^p}{\alpha} \quad (92)$$

$$= D_\alpha(p||\nu) + \gamma_\alpha^p D_\alpha(\nu||q) + \frac{\gamma_\alpha^p}{\alpha} \quad (93)$$

and duality with $\alpha < 0$ (hence, $1 - \alpha > 1$)

$$D_\alpha(p||q) = D_{1-\alpha}(q||p) \quad (94)$$

$$\leq \gamma_\alpha^p D_{1-\alpha}(q||\nu) + D_{1-\alpha}(\nu||p) - \frac{\gamma_\alpha^p}{\alpha} \quad (95)$$

$$= D_\alpha(p||\nu) + \gamma_\alpha^p D_\alpha(\nu||q) + \left| \frac{\gamma_\alpha^p}{\alpha} \right| \quad (96)$$

Next, for $\alpha = 1$.

$$\phi_\alpha \left(\frac{p}{q} \right) = \frac{p}{q} \log \left(\frac{p}{\nu} \right) + \frac{p\nu}{\nu q} \log \left(\frac{\nu}{q} \right) - \frac{p}{q} + 1 \quad (97)$$

$$= \frac{p}{q} \log \left(\frac{p}{\nu} \right) + \frac{p}{\nu} \phi_\alpha \left(\frac{\nu}{q} \right) + \frac{\nu}{q} - \frac{p}{q} \quad (98)$$

Inserting for D_{KL} ,

$$D_{\text{KL}}(p||q) \leq D_{\text{KL}}(p||\nu) + \sup \frac{p}{\nu} D_{\text{KL}}(\nu||q) + 1 - 1 \quad (99)$$

$$\leq D_{\text{KL}}(p||\nu) + \gamma_\alpha^p D_{\text{KL}}(\nu||q) \quad (100)$$

We do $\alpha = 0$ by duality

$$D_0(p||q) = D_{\text{KL}}(q||p) \quad (101)$$

$$\leq D_{\text{KL}}(q||\nu) + \gamma_1^q D_{\text{KL}}(\nu||p) \quad (102)$$

$$= \gamma_{1-\alpha}^q D_0(p||\nu) + D_0(\nu||q). \quad (103)$$

A.5 Proof of Proposition 3

Let us first work with normalized densities. We have to assume that $\alpha \geq 1$. Note that $\beta \geq \gamma_\alpha^{\pi^\ell}$ in Proposition 2.

$$D_\alpha(\pi^{(L)}||\tilde{\pi}^{(L)}) \stackrel{\text{Ass. 1}}{\leq} \omega D_\alpha(\pi^{(L)}||\tilde{\pi}^{(L-1)}) \quad (104)$$

$$\stackrel{\text{Prop. 2}}{\leq} \omega \left[D_\alpha(\pi^{(L)}||\pi^{(L-1)}) + \beta D_\alpha(\pi^{(L-1)}||\tilde{\pi}^{(L-1)}) + \frac{\beta}{\alpha} \right]. \quad (105)$$

By recursion and $D_\alpha(\pi^{(0)}||\tilde{\pi}^{(0)}) = 0$, we get

$$D_\alpha(\pi^{(L)}||\tilde{\pi}^{(L)}) \leq \omega \sum_{i=1}^L (\omega\beta)^{L-i} \left[D_\alpha(\pi^{(i)}||\pi^{(i-1)}) + \frac{\beta}{\alpha} \right] \quad (106)$$

$$\stackrel{\text{Def. 1}}{\leq} \omega \sum_{i=1}^L (\omega\beta)^{L-i} \left[\eta(L) + \frac{\beta}{\alpha} \right] \quad (107)$$

$$\leq \omega \left[\eta(L) + \frac{\beta}{\alpha} \right] + \omega \sum_{i=1}^{L-1} (\omega\beta)^i \left[\eta(L) + \frac{\beta}{\alpha} \right] \quad (108)$$

$$\stackrel{\omega\beta < 1}{\leq} \omega \left[\eta(L) + \frac{\beta}{\alpha} \right] + \frac{\omega^2\beta}{1-\omega\beta} \left[\eta(L) + \frac{\beta}{\alpha} \right] \quad (109)$$

$$\leq \frac{\omega\beta}{1-\omega\beta} \left[\eta(L) + \frac{\beta}{\alpha} \right]. \quad (110)$$

A.6 Proof of Proposition 4

Let $\tilde{\pi}^{(0)} = \pi^{(0)}$, e.g. by setting $\pi^{(0)} = \rho_{\text{ref}}$ or with a known diagonal map $\mathcal{R}_0^\# \pi^{(0)} = \mu$, so that $\tilde{\pi}^{(0)}$ can be build exactly.

$$\begin{aligned}
D_\alpha(\pi^{(L)} || \tilde{\pi}^{(L)}) &\stackrel{\text{Ass. 1}}{\leq} \omega D_\alpha(\pi^{(L)} || \tilde{\pi}^{(L-1)}) \\
&\stackrel{\text{Pythag.}}{=} \omega \left[D_\alpha(\pi^{(L)} || f_{\text{proj}}^{(L)}) + D_\alpha(f_{\text{proj}}^{(L)} || \tilde{\pi}^{(L-1)}) \right] \\
&\stackrel{\text{Ass. 3}}{\leq} \omega(1 + \epsilon) D_\alpha(\pi^{(L)} || \pi^{(L-1)}) + \omega D_\alpha(f_{\text{proj}}^{(L)} || \tilde{\pi}^{(L-1)}) \\
&\stackrel{\text{Eq. (57)}}{\leq} \omega(1 + \epsilon) D_\alpha(\pi^{(L)} || \pi^{(L-1)}) + \omega D_\alpha(\pi^{(L-1)} || \tilde{\pi}^{(L-1)})
\end{aligned}$$

By recursion,

$$\begin{aligned}
D_\alpha(\pi^{(L)} || \tilde{\pi}^{(L)}) &\leq \omega(1 + \epsilon) \sum_{\ell=1}^L \omega^{L-\ell} D_\alpha(\pi^{(\ell)} || \pi^{(\ell-1)}) + \omega^L D_\alpha(\pi^{(0)} || \tilde{\pi}^{(0)}) \\
&= \omega(1 + \epsilon) \sum_{\ell=1}^L \omega^{L-\ell} D_\alpha(\pi^{(\ell)} || \pi^{(\ell-1)}) \\
&\stackrel{\text{Def. 1}}{\leq} \omega(1 + \epsilon) \sum_{\ell=1}^L \omega^{L-\ell} \eta(L) \\
&\leq \omega(1 + \epsilon) \eta(L) + \omega(1 + \epsilon) \sum_{\ell=1}^{L-1} \omega^\ell \eta(L) \\
&= \omega(1 + \epsilon) \sum_{\ell=0}^{L-1} \omega^\ell \eta(L) \\
&\leq \frac{\omega(1 + \epsilon)}{1 - \omega} \eta(L)
\end{aligned}$$

A.7 Proof of Remark 4.2 and Remark 4.6

First, we translate the variables used in [10] to the ones used in this paper. We call the variables from [10] ω_H and η_H , defined by

$$D_{\text{Hell}}(\pi^{(\ell)} || \tilde{\pi}^{(\ell)}) \leq \omega_H D_{\text{Hell}}(\pi^{(\ell)} || \tilde{\pi}^{(\ell-1)}) \quad (111)$$

and

$$D_{\text{Hell}}(\pi^{(\ell)} || \pi^{(\ell-1)}) \leq \eta_H \quad \forall \ell \in [L]. \quad (112)$$

We translate, using $\alpha = 0.5$,

$$D_\alpha(\pi^{(\ell)} || \tilde{\pi}^{(\ell)}) \leq \omega D_\alpha(\pi^{(\ell)} || \tilde{\pi}^{(\ell-1)}) \quad (113)$$

$$4 D_{\text{Hell}}(\pi^{(\ell)} || \tilde{\pi}^{(\ell)})^2 \leq \omega 4 D_{\text{Hell}}(\pi^{(\ell)} || \tilde{\pi}^{(\ell-1)})^2 \quad (114)$$

$$D_{\text{Hell}}(\pi^{(\ell)} || \tilde{\pi}^{(\ell)})^2 \leq \sqrt{\omega} D_{\text{Hell}}(\pi^{(\ell)} || \tilde{\pi}^{(\ell-1)}), \quad (115)$$

hence, $\omega_H = \sqrt{\omega}$ (equal sign by doing the reverse and $\omega_H \leq \sqrt{\omega} \leq \omega_H$), and

$$D_\alpha (\pi^{(\ell)} || \pi^{(\ell-1)}) \leq \eta \quad (116)$$

$$4 D_{\text{Hell}} (\pi^{(\ell)} || \pi^{(\ell-1)})^2 \leq \eta \quad (117)$$

$$D_{\text{Hell}} (\pi^{(\ell)} || \pi^{(\ell-1)}) \leq \frac{1}{2} \sqrt{\eta}, \quad (118)$$

hence, $\eta_H = \frac{1}{2} \sqrt{\eta}$ (same as before to get the equality). Therefore, the bound given in [10] writes

$$D_{\text{Hell}} (\pi^{(L)} || \tilde{\pi}^{(L)}) \leq \frac{\omega_H}{1 - \omega_H} \eta_H = \frac{1}{2} \frac{\sqrt{\omega}}{1 - \sqrt{\omega}} \sqrt{\eta}. \quad (119)$$

Let us show that the bound derived by the geometric properties is strictly better compared to the bound in [10]. Note that for $0 < \omega < 1$, $\omega \leq \sqrt{\omega}$.

$$\frac{1}{2} \sqrt{\frac{\omega}{1 - \omega}} \sqrt{\eta} \leq \frac{1}{2} \frac{\sqrt{\omega}}{1 - \sqrt{\omega}} \sqrt{\eta} \quad (120)$$

$$\frac{\sqrt{\omega}}{\sqrt{1 - \omega}} \leq \frac{\sqrt{\omega}}{1 - \sqrt{\omega}} \quad (121)$$

$$1 - \sqrt{\omega} \leq \sqrt{1 - \omega} \quad (122)$$

$$1 - 2\sqrt{\omega} + \omega \leq 1 - \omega \quad (123)$$

$$1 - 2\sqrt{\omega} + \omega \leq 1 - 2\omega + \omega = 1 - \omega. \quad (124)$$

Equality holds for $\omega \rightarrow 0, 1$.

B Comparison of the KL divergence for positive measures and probability distributions

In [16], the paper is motivated in the appendix by the fact that a naive discretization of the KL divergence does not converge to the true density and is unstable. In a naive discretization, the minimization problem

$$\min_{\tilde{\pi}} D_{\text{KL}}(\pi || \tilde{\pi})$$

is discretized by

$$\begin{aligned} \min_{\tilde{\pi}} D_{\text{KL}}(\pi || \tilde{\pi}) &= \min_{\tilde{\pi}} - \int \log(\tilde{\pi}) d\pi \\ &\approx \min_{\tilde{\pi}} - \sum_i \log(\tilde{\pi}(x^i)) \frac{\pi(x^i)}{p(x^i)} \quad x^i \sim p \end{aligned}$$

with a distribution p used for importance sampling. The authors consider a gradient descent approach, in which the gradient

$$\frac{d\tilde{\pi}}{dt} = -\nabla_{\tilde{\pi}} D_{\text{KL}}(\pi || \tilde{\pi})$$

of the discretized KL divergence is followed. Hence, we can calculate this evaluated at a single discretization point x^i ,

$$\frac{d\tilde{\pi}}{dt}\Big|_{x=x^i} = \frac{\pi}{\tilde{\pi}}\Big|_{x=x^i}.$$

A solution to this is (see [16])

$$\tilde{\pi}(x^i) = \sqrt{2t\pi(x^i)}.$$

Hence, it is necessary to satisfy $\int d\tilde{\pi} = 1$ in order to converge to π (see [16]). We show that for the extension of the KL divergence, gradient descent converges for any single point x^i to $\pi(x^i)$. Note that

$$\begin{aligned}\nabla_{\tilde{\pi}} D_{\text{KL}}(\pi||\tilde{\pi}) &= - \int \frac{\pi}{\tilde{\pi}} dx - \int dx \\ \nabla_{\tilde{\pi}} D_{\text{KL}}(\pi||\tilde{\pi})\Big|_{x=x^i} &= \frac{\pi(x^i)}{\tilde{\pi}(x^i)} - 1.\end{aligned}$$

While before, for $\pi, \tilde{\pi} > 0$ the gradient never reached 0, here, the minima is reached for $\pi(x^i) = \tilde{\pi}(x^i)$.

C A Heuristic for choosing the timesteps in the inverse diffusion process

In the following, we try to find optimal time steps in the reversed Ornstein-Uhlenbeck process so that β from Assumption 2 is small. First, note that we can bound the $\|\bullet\|_{\infty}$ of π_t in the Ornstein-Uhlenbeck process.

Proposition 5 (Bound on $\|\bullet\|_{\infty}$ for Ornstein-Uhlenbeck process). Let $\pi^{(0)} = \rho_{\text{ref}}$ be the stationary solution of the Ornstein-Uhlenbeck process and π a normalized distribution. We have that

$$\|\pi_t(x)\|_{\infty} \leq \frac{1}{(2\pi(1 - e^{-2t}))^{d/2}}$$

where π_t as in Eq. (41).

Proof. Using Young's convolution inequality

$$\|\pi \star \kappa_t\|_{\infty} \leq \|\pi\|_1 \|\kappa_t\|_{\infty}. \quad (125)$$

Because we assume probability densities, $\|\pi\|_1 = \|\kappa_t\|_1 = 1$. We can calculate $\|\kappa_t(y)\|_{\infty}$, since it is a Gaussian pdf:

$$\|\kappa_t\|_{\infty} = \frac{1}{(2\pi(1 - e^{-2t}))^{d/2}}.$$

□

Note that in general this bound is not tight. Nevertheless, it gives a decay of the maximum value of the distribution in the diffusion process and we use it as an heuristic. We need to work with an assumption that for small t the bound is less tight compared to larger t .

Assumption 4. Define a constant $C_t \leq 1$, so that

$$\|\pi_t(x)\|_\infty = C_t \frac{1}{(2\pi(1 - e^{-2t}))^{d/2}}. \quad (126)$$

We make the assumption that $C_{t_1} \leq C_{t_2}$ for $t_1 \leq t_2$.

We are not able to bound β , but instead to bound a variable $\tilde{\beta} = \frac{\|\pi^{(\ell+1)}\|_\infty}{\|\pi^{(\ell)}\|_\infty}$ which is a lower bound of β and assume that $\beta \approx \tilde{\beta}$.

Proposition 6 ($\tilde{\beta}$ is a lower bound of β). $\tilde{\beta} = \frac{\|\pi^{(\ell+1)}\|_\infty}{\|\pi^{(\ell)}\|_\infty} \forall \ell \in [L]$ is a lower bound of β .

Proof.

$$\beta = \sup_{x \in \mathcal{X}} \frac{\pi^{(\ell+1)}}{\pi^{(\ell)}} \geq \sup_{x \in \mathcal{X}} \frac{\pi^{(\ell+1)}}{\|\pi^{(\ell)}\|_\infty} = \frac{\|\pi^{(\ell+1)}\|_\infty}{\|\pi^{(\ell)}\|_\infty} = \tilde{\beta}.$$

□

With these, we are able to choose a timestep $t_{\ell+1}$ given t_ℓ so that $\tilde{\beta}$ is smaller than some given value.

Corollary 2 (Bound on $\tilde{\beta}$ by diffusion process). Given t_ℓ and $\tilde{\beta}$, assuming Assumption 4 holds, a subsequent time step $t_{\ell+1}$ so that $\frac{\|\pi^{(\ell+1)}\|_\infty}{\|\pi^{(\ell)}\|_\infty} \leq \tilde{\beta}$ is satisfied for

$$t_{\ell+1} \geq -\frac{1}{2} \ln \left(1 - \frac{1 - \exp(-2t_\ell)}{\tilde{\beta}^{2/d}} \right).$$

Proof. Given $\tilde{\beta}$ and t_ℓ , we want to find $t_{\ell+1}$. Note that $t_{\ell+1} \leq t_\ell$ and therefore, from Assumption 4, $C_{t_{\ell+1}} \leq C_{t_\ell}$. This gives

$$\tilde{\beta} = \frac{\|\pi^{(\ell+1)}\|_\infty}{\|\pi^{(\ell)}\|_\infty} = \frac{C_{t_{\ell+1}} [2\pi(1 - \exp(-2t_\ell))]^{d/2}}{C_{t_\ell} [2\pi(1 - \exp(-2t_{\ell+1}))]^{d/2}} \stackrel{\text{Ass. 4}}{\leq} \frac{[2\pi(1 - \exp(-2t_\ell))]^{d/2}}{[2\pi(1 - \exp(-2t_{\ell+1}))]^{d/2}}$$

$$\tilde{\beta}(1 - e^{-2t_{\ell+1}})^{d/2} \geq (1 - e^{-2t_\ell})^{d/2}$$

$$1 - e^{-2t_{\ell+1}} \geq \frac{1}{\tilde{\beta}^{2/d}}(1 - e^{-2t_\ell})$$

$$e^{-2t_{\ell+1}} \leq 1 - \frac{1 - e^{-2t_\ell}}{\tilde{\beta}^{2/d}}$$

$$t_{\ell+1} \geq -\frac{1}{2} \ln \left(1 - \frac{1 - e^{-2t_\ell}}{\tilde{\beta}^{2/d}} \right).$$

□

D Implementation details

We implement our method in Julia. To optimize the SoS functions, we use the *JuMP.jl* library [24], an interface for implementing SDP and other optimization problems. As a solver, we use *Hypatia.jl* [6], an interior point solver.

Next, we explain in more details how the minimization of α -divergences is performed using SDP. First, we discretize α -divergences using evaluations at $x^i \sim \mu$, so that

$$\min_g D_\alpha(f||g) = \min_g \int \phi_\alpha\left(\frac{f}{g}\right) dg \quad (127)$$

$$= \min_g \int \frac{f^\alpha g^{1-\alpha} - g}{\alpha(\alpha-1)} - \frac{f-g}{\alpha-1} d\mu \quad (128)$$

$$= \min_g \int \frac{f^\alpha g^{1-\alpha}}{\alpha(\alpha-1)} + \frac{g}{\alpha} d\mu \quad (129)$$

$$= \min_g \frac{1}{N} \sum_{i=1}^N \frac{f(x^i)^\alpha g(x^i)^{1-\alpha}}{\alpha(\alpha-1)} + \int \frac{g}{\alpha} d\mu \quad \text{with } x^i \sim \mu. \quad (130)$$

g itself is an SoS-function, where $A \succeq 0$. This is handled in SDP by using a PSD cone for A . To integrate $\int g/\alpha d\mu$, we use that $\int g d\mu = \text{trace}(A)$. The main difficulty remaining is to map $g(x^i)^{1-\alpha}$ to an SDP problem. To do so, we use an auxiliary variable t_i , so that t_i upper or lower bounds $f(x^i)^\alpha g(x^i)^{1-\alpha}$ and minimize over this variable at the same time.

For this, we use the power cone for $\alpha \neq 0, 1$, given by

$$K_p = \{(x, y, z) \in \mathbb{R}^3 : x^p y^{1-p} \geq |z|, x \geq 0, y \geq 0\}. \quad (131)$$

First, consider $\alpha < 0$. We use another variable t_i , so that $t_i \geq f(x^i)^\alpha g(x^i)^{1-\alpha}$ and write

$$t_i \geq f(x^i)^\alpha g(x^i)^{1-\alpha} \quad (132)$$

$$t_i f(x^i)^{-\alpha} \geq g(x^i)^{1-\alpha} \quad (133)$$

$$t_i^{\frac{1}{1-\alpha}} (f(x^i)^{-1})^{\frac{\alpha}{1-\alpha}} \geq g(x^i). \quad (134)$$

Since $f(x^i)^{-1}$ can be very high, for numerical reasons it is better to use

$$t_i^{\frac{1}{1-\alpha}} \geq f(x^i)^{\frac{\alpha}{1-\alpha}} g(x^i) \quad (135)$$

and map this to the powercone with $(t_i, 1, f(x^i)^{\frac{\alpha}{1-\alpha}} g(x^i)) \in K_{1/(1-\alpha)}$.

Next, we consider $0 < \alpha < 1$. Note, that $\alpha(\alpha-1)$ is negative in this region, hence, we use a variable t_i , so that $t_i \leq f(x^i)^\alpha g(x^i)^{1-\alpha}$. This directly maps to the powercone, by using $(f(x^i), g(x^i), t_i) \in K_\alpha$.

Last, we consider $\alpha > 1$ and again we seek for $t_i \geq f(x^i)^\alpha g(x^i)^{1-\alpha}$ but we can not use the same formulation as for $\alpha < 0$, since in the powercone $p \in [0, 1]$. Hence, we formulate

$$t_i \geq f(x^i)^\alpha g(x^i)^{1-\alpha} \quad (136)$$

$$t_i g(x^i)^{\alpha-1} \geq f(x^i)^\alpha \quad (137)$$

$$t_i^{\frac{1}{\alpha}} g(x^i)^{1-\frac{1}{\alpha}} \geq f(x^i). \quad (138)$$

This maps to the powercone as $(t_i, g(x^i), f(x^i)) \in K_{1/\alpha}$.

For $\alpha = 0, 1$, the powercone does not work. Instead, the exponential cone could be used. However, *JuMP* has the possibility of using the *relative entropy cone*, which directly works with the *Hypatia.jl* solver. This cone is given by

$$K_n = \left\{ (u, v, w) \in \mathbb{R}^{1+2n} \mid u \geq \sum_{i=1}^n w_i \log \left(\frac{w_i}{v_i} \right) \right\}. \quad (139)$$

Both the KL divergence, as well as the reverse KL divergence, can be implemented using this cone.

References

- [1] Shun-ichi Amari. *Information Geometry and Its Applications*. en. Vol. 194. Applied Mathematical Sciences. Tokyo: Springer Japan, 2016. ISBN: 978-4-431-55977-1 978-4-431-55978-8. DOI: 10.1007/978-4-431-55978-8. URL: <http://link.springer.com/10.1007/978-4-431-55978-8> (visited on 08/31/2023).
- [2] Ricardo Baptista, Michael C Brennan, and Youssef Marzouk. “Dimension reduction via score ratio matching”. en. In: (2022).
- [3] Ricardo Baptista, Youssef Marzouk, and Olivier Zahm. “On the representation and learning of monotone triangular transport maps”. In: *Foundations of Computational Mathematics* (2023), pp. 1–46.
- [4] Michael C Brennan et al. “Greedy inference with structure-exploiting lazy maps”. en. In: *34th Conference on Neural Information Processing Systems*. 2020.
- [5] Andrzej Cichocki and Shun-ichi Amari. “Families of Alpha- Beta- and Gamma-Divergences: Flexible and Robust Measures of Similarities”. en. In: *Entropy* 12.6 (June 2010), pp. 1532–1568. ISSN: 1099-4300. DOI: 10.3390/e12061532. URL: <http://www.mdpi.com/1099-4300/12/6/1532> (visited on 09/01/2023).
- [6] Chris Coey, Lea Kapelevich, and Juan Pablo Vielma. “Solving natural conic formulations with Hypatia.jl”. In: *INFORMS Journal on Computing* 34.5 (2022), pp. 2686–2699. DOI: <https://doi.org/10.1287/ijoc.2022.1202>.
- [7] Albert Cohen and Giovanni Migliorati. “Multivariate Approximation in Downward Closed Polynomial Spaces”. In: *Contemporary Computational Mathematics - A Celebration of the 80th Birthday of Ian Sloan*. Ed. by Josef Dick, Frances Y. Kuo, and Henryk Woźniakowski. Cham: Springer International Publishing, 2018, pp. 233–282. ISBN: 978-3-319-72456-0. DOI: 10.1007/978-3-319-72456-0_12. URL: https://doi.org/10.1007/978-3-319-72456-0_12.
- [8] Tiangang Cui and Sergey Dolgov. “Deep composition of tensor-trains using squared inverse Rosenblatt transports”. en. In: *Foundations of Computational Mathematics* (Sept. 2021). arXiv:2007.06968 [cs, math, stat]. ISSN: 1615-3375, 1615-3383. DOI: 10.1007/s10208-021-09537-5. URL: <http://arxiv.org/abs/2007.06968> (visited on 07/19/2022).
- [9] Tiangang Cui, Sergey Dolgov, and Robert Scheichl. “Deep Importance Sampling Using Tensor Trains with Application to a Priori and a Posteriori Rare Events”. In: *SIAM Journal on Scientific Computing* 46.1 (2024), pp. C1–C29.

- [10] Tiangang Cui, Sergey Dolgov, and Olivier Zahm. “Scalable conditional deep inverse Rosenblatt transports using tensor trains and gradient-based dimension reduction”. In: *Journal of Computational Physics* 485 (2023), p. 112103. ISSN: 0021-9991. DOI: <https://doi.org/10.1016/j.jcp.2023.112103>. URL: <https://www.sciencedirect.com/science/article/pii/S0021999123001985>.
- [11] Tiangang Cui, Sergey Dolgov, and Olivier Zahm. *Self-reinforced polynomial approximation methods for concentrated probability densities*. en. arXiv:2303.02554 [cs, math, stat]. Mar. 2023. URL: <http://arxiv.org/abs/2303.02554> (visited on 03/20/2023).
- [12] Pierre Del Moral, Arnaud Doucet, and Ajay Jasra. “Sequential monte carlo samplers”. In: *Journal of the Royal Statistical Society Series B: Statistical Methodology* 68.3 (2006), pp. 411–436.
- [13] Pierre Del Moral, Arnaud Doucet, and Ajay Jasra. “Sequential Monte Carlo Samplers”. en. In: *Journal of the Royal Statistical Society Series B: Statistical Methodology* 68.3 (June 2006), pp. 411–436. ISSN: 1369-7412, 1467-9868. DOI: 10.1111/j.1467-9868.2006.00553.x. URL: <https://academic.oup.com/jrsssb/article/68/3/411/7110641> (visited on 02/12/2024).
- [14] Laurent Dinh, Jascha Sohl-Dickstein, and Samy Bengio. *Density estimation using Real NVP*. en. arXiv:1605.08803 [cs, stat]. Feb. 2017. URL: <http://arxiv.org/abs/1605.08803> (visited on 12/01/2023).
- [15] Sergey Dolgov et al. “Approximation and sampling of multivariate probability distributions in the tensor train decomposition”. In: *Statistics and Computing* 30 (2020), pp. 603–625.
- [16] Loris Felardos, Jérôme Hénin, and Guillaume Charpiat. *Designing losses for data-free training of normalizing flows on Boltzmann distributions*. en. arXiv:2301.05475 [cond-mat]. Jan. 2023. URL: <http://arxiv.org/abs/2301.05475> (visited on 04/24/2023).
- [17] Michael Grant and Stephen Boyd. *CVX: Matlab Software for Disciplined Convex Programming, version 2.1*. <https://cvxr.com/cvx>. Mar. 2014.
- [18] Louis Grenioux et al. “On Sampling with Approximate Transport Maps”. In: *arXiv preprint arXiv:2302.04763* (2023).
- [19] Priyank Jaini, Kira A Selby, and Yaoliang Yu. “Sum-of-squares polynomial flow”. In: *International Conference on Machine Learning*. PMLR. 2019, pp. 3009–3018.
- [20] William Ogilvy Kermack, A. G. McKendrick, and Gilbert Thomas Walker. “A contribution to the mathematical theory of epidemics”. In: *Proceedings of the Royal Society of London. Series A, Containing Papers of a Mathematical and Physical Character* 115.772 (1927). eprint: <https://royalsocietypublishing.org/doi/pdf/10.1098/rspa.1927.0118>, pp. 700–721. DOI: 10.1098/rspa.1927.0118. URL: <https://royalsocietypublishing.org/doi/abs/10.1098/rspa.1927.0118>.
- [21] Tom H. Koornwinder. “Orthogonal polynomials, a short introduction”. en. In: arXiv:1303.2825 [math]. 2013, pp. 145–170. DOI: 10.1007/978-3-7091-1616-6_6. URL: <http://arxiv.org/abs/1303.2825> (visited on 02/16/2024).

- [22] Jean-Bernard Lasserre. *Moments, positive polynomials and their applications*. en. Imperial College Press optimization series v. 1. OCLC: ocn503631126. London : Signapore ; Hackensack, NJ: Imperial College Press ; Distributed by World Scientific Publishing Co, 2010. ISBN: 978-1-84816-445-1.
- [23] Steffen L. Lauritzen. *Graphical models*. Oxford statistical science series 17. Oxford : New York: Clarendon Press ; Oxford University Press, 1996. ISBN: 978-0-19-852219-5.
- [24] Miles Lubin et al. “JuMP 1.0: Recent improvements to a modeling language for mathematical optimization”. In: *Mathematical Programming Computation* (2023). DOI: 10.1007/s12532-023-00239-3.
- [25] Ulysse Marteau-Ferey, Francis Bach, and Alessandro Rudi. “Non-Parametric Models for Non-Negative Functions”. In: *Proceedings of the 34th International Conference on Neural Information Processing Systems*. NIPS’20. event-place: Vancouver, BC, Canada. Red Hook, NY, USA: Curran Associates Inc., 2020. ISBN: 978-1-71382-954-6.
- [26] Youssef Marzouk et al. “An introduction to sampling via measure transport”. en. In: arXiv:1602.05023 [math, stat]. 2016, pp. 1–41. DOI: 10.1007/978-3-319-11259-6_23-1. URL: <http://arxiv.org/abs/1602.05023> (visited on 07/20/2022).
- [27] Thomas Minka. “Divergence measures and message passing”. en. In: *Microsoft Research Technical Report* (2005).
- [28] Frank Nielsen. “An elementary introduction to information geometry”. en. In: *Entropy* 22.10 (Sept. 2020). arXiv:1808.08271 [cs, math, stat], p. 1100. ISSN: 1099-4300. DOI: 10.3390/e22101100. URL: <http://arxiv.org/abs/1808.08271> (visited on 09/19/2023).
- [29] Frank Noé et al. “Boltzmann generators: Sampling equilibrium states of many-body systems with deep learning”. In: *Science* 365.6457 (2019), eaaw1147.
- [30] George Papamakarios et al. *Normalizing Flows for Probabilistic Modeling and Inference*. en. arXiv:1912.02762 [cs, stat]. Apr. 2021. URL: <http://arxiv.org/abs/1912.02762> (visited on 05/22/2023).
- [31] Matthew D Parno and Youssef M Marzouk. “Transport map accelerated markov chain monte carlo”. In: *SIAM/ASA Journal on Uncertainty Quantification* 6.2 (2018), pp. 645–682.
- [32] Gabriel Peyré, Marco Cuturi, et al. “Computational optimal transport: With applications to data science”. In: *Foundations and Trends® in Machine Learning* 11.5-6 (2019), pp. 355–607.
- [33] Mihai Putinar. “Positive Polynomials on Compact Semi-algebraic Sets”. In: *Indiana University Mathematics Journal* 42.3 (1993). Publisher: Indiana University Mathematics Department, pp. 969–984. ISSN: 00222518, 19435258. URL: <http://www.jstor.org/stable/24897130> (visited on 12/01/2023).
- [34] Danilo Rezende and Shakir Mohamed. “Variational inference with normalizing flows”. In: *International conference on machine learning*. PMLR. 2015, pp. 1530–1538.

- [35] Danilo Jimenez Rezende and Shakir Mohamed. *Variational Inference with Normalizing Flows*. en. arXiv:1505.05770 [cs, stat]. June 2016. URL: <http://arxiv.org/abs/1505.05770> (visited on 06/13/2023).
- [36] Murray Rosenblatt. “Remarks on a Multivariate Transformation”. In: *The Annals of Mathematical Statistics* 23.3 (1952), pp. 470–472. DOI: 10.1214/aoms/1177729394.
- [37] Jonathan Schwarz et al. “Riemannian SOS-Polynomial Normalizing Flows”. en. In: *Pattern Recognition*. Ed. by Zeynep Akata, Andreas Geiger, and Torsten Sattler. Vol. 12544. Series Title: Lecture Notes in Computer Science. Cham: Springer International Publishing, 2021, pp. 218–231. ISBN: 978-3-030-71277-8 978-3-030-71278-5. DOI: 10.1007/978-3-030-71278-5_16. URL: https://link.springer.com/10.1007/978-3-030-71278-5_16 (visited on 06/12/2023).
- [38] Jie Shen, Li-Lian Wang, and Haijun Yu. “Approximations by orthonormal mapped Chebyshev functions for higher-dimensional problems in unbounded domains”. en. In: *Journal of Computational and Applied Mathematics* 265 (Aug. 2014), pp. 264–275. ISSN: 03770427. DOI: 10.1016/j.cam.2013.09.024. URL: <https://linkinghub.elsevier.com/retrieve/pii/S0377042713004792> (visited on 05/16/2023).
- [39] Jascha Sohl-Dickstein et al. “Deep unsupervised learning using nonequilibrium thermodynamics”. In: *International conference on machine learning*. PMLR. 2015, pp. 2256–2265.
- [40] Yang Song et al. “Score-Based Generative Modeling through Stochastic Differential Equations”. In: *International Conference on Learning Representations*. 2021. URL: <https://openreview.net/forum?id=PxTIG12RRHS>.
- [41] Alessio Spantini, Daniele Bigoni, and Youssef Marzouk. *Inference via low-dimensional couplings*. en. arXiv:1703.06131 [stat]. July 2018. URL: <http://arxiv.org/abs/1703.06131> (visited on 09/15/2023).
- [42] Benigno Uria, Iain Murray, and Hugo Larochelle. *RNADE: The real-valued neural autoregressive density-estimator*. en. arXiv:1306.0186 [cs, stat]. Jan. 2014. URL: <http://arxiv.org/abs/1306.0186> (visited on 10/10/2023).
- [43] Cédric Villani et al. *Optimal transport: old and new*. Vol. 338. Springer, 2009.
- [44] Josephine Westermann and Jakob Zech. *Measure transport via polynomial density surrogates*. en. arXiv:2311.04172 [cs, math, stat]. Nov. 2023. URL: <http://arxiv.org/abs/2311.04172> (visited on 12/01/2023).
- [45] Huaiyu Zhu and Richard Rohwer. “Bayesian invariant measurements of generalization”. en. In: *Neural Processing Letters* 2.6 (Dec. 1995), pp. 28–31. ISSN: 1370-4621, 1573-773X. DOI: 10.1007/BF02309013. URL: <http://link.springer.com/10.1007/BF02309013> (visited on 12/07/2023).